Cell Reports

Resource

Extensive remodeling of the extracellular matrix during aging contributes to age-dependent impairments of muscle stem cell functionality

Graphical abstract

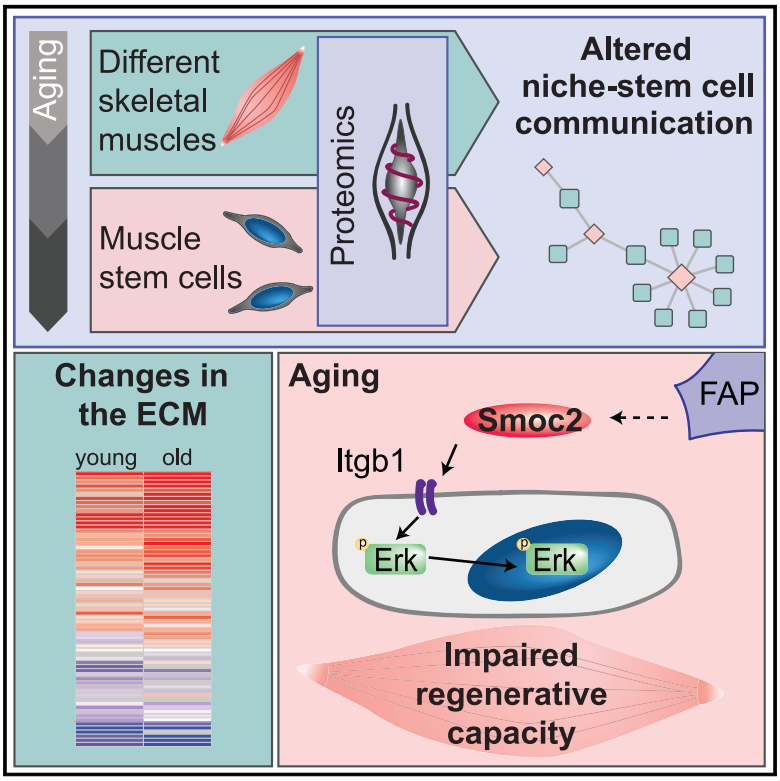

Authors

Svenja C. Schüler, Joanna M. Kirkpatrick, Manuel Schmidt, ..., Martin Hemberg, Alessandro Ori, Julia von Maltzahn

Correspondence

alessandro.ori@leibniz-fli.de (A.O.), julia.vonmaltzahn@leibniz-fli.de (J.v.M.)

In brief

Schüler et al. describe aging-dependent changes in the proteome of muscle stem cells and their niche. They also demonstrate that those age-dependent changes in the niche impair muscle stem cell functionality and thereby regeneration of skeletal muscle.

Highlights

- Proteomes of aged MuSCs and skeletal muscles reveal altered communication
- 183 extracellular proteins change abundance in different skeletal muscles during aging
- FAPs are the main source of niche proteins affected during aging
- Injection of Smoc2 into regenerating muscle of young mice hampers regeneration

Schüler et al., 2021, Cell Reports *35*, 109223
June 8, 2021
https://doi.org/10.1016/j.celrep.2021.109223

CellPress

Cell Reports

CellPress
OPEN ACCESS

Resource

Extensive remodeling of the extracellular matrix during aging contributes to age-dependent impairments of muscle stem cell functionality

Svenja C. Schüler,[1] Joanna M. Kirkpatrick,[1,5,6] Manuel Schmidt,[1,5] Deolinda Santinha,[2] Philipp Koch,[1] Simone Di Sanzo,[1] Emilio Cirri,[1] Martin Hemberg,[3] Alessandro Ori,[1,4,*] and Julia von Maltzahn[1,4,7,*]

[1]Leibniz Institute on Aging, Fritz Lipmann Institute, Beutenbergstrasse 11, 07745 Jena, Germany
[2]Faculty of Medicine and Center for Neuroscience and Cell Biology, University of Coimbra, Rua Larga, 3004-504 Coimbra, Portugal
[3]Wellcome Sanger Institute, Wellcome Genome Campus, Hinxton CB10 1SA, UK
[4]Senior author
[5]These authors contributed equally
[6]Present address: Proteomics Science Technology Platform, The Francis Crick Institute, London, UK
[7]Lead contact
*Correspondence: alessandro.ori@leibniz-fli.de (A.O.), julia.vonmaltzahn@leibniz-fli.de (J.v.M.)
https://doi.org/10.1016/j.celrep.2021.109223

SUMMARY

During aging, the regenerative capacity of skeletal muscle decreases due to intrinsic changes in muscle stem cells (MuSCs) and alterations in their niche. Here, we use quantitative mass spectrometry to characterize intrinsic changes in the MuSC proteome and remodeling of the MuSC niche during aging. We generate a network connecting age-affected ligands located in the niche and cell surface receptors on MuSCs. Thereby, we reveal signaling by integrins, Lrp1, Egfr, and Cd44 as the major cell communication axes perturbed through aging. We investigate the effect of Smoc2, a secreted protein that accumulates with aging, primarily originating from fibro-adipogenic progenitors. Increased levels of Smoc2 contribute to the aberrant Integrin beta-1 (Itgb1)/mitogen-activated protein kinase (MAPK) signaling observed during aging, thereby causing impaired MuSC functionality and muscle regeneration. By connecting changes in the proteome of MuSCs to alterations of their niche, our work will enable a better understanding of how MuSCs are affected during aging.

INTRODUCTION

Skeletal muscle possesses a remarkable ability to regenerate (Schmidt et al., 2019), a process that depends on muscle stem cells (MuSCs)—also termed satellite cells (Lepper et al., 2011; Murphy et al., 2011; Sambasivan et al., 2011). MuSCs are quiescent in resting skeletal muscle and can be identified by the expression of the transcription factor Pax7 (Sousa-Victor et al., 2015). Stimuli like injury lead to the activation of MuSCs coinciding with increased expression of Myf5 and MyoD (Chang and Rudnicki, 2014; Schmidt et al., 2019). This is followed by a tightly controlled sequence of myogenic transcription factors that resembles myogenesis during embryonic development required for myogenic progression (Bentzinger et al., 2012; Price et al., 2014; Schmidt et al., 2019).

MuSCs interact with their immediate cellular environment, also known as the stem cell niche. The interaction with the niche is critical to provide MuSCs with the proper cues for self-renewal, proliferation, and differentiation (Bentzinger et al., 2013a; Wosczyna and Rando, 2018). A major component of the MuSC niche is the extracellular matrix (ECM), which is remodeled by various cell types during regeneration (Evano and Tajbakhsh, 2018). Multiple studies have demonstrated the critical role of ECM components for MuSC functionality (Baghdadi et al., 2018; Brack et al., 2007; Lukjanenko et al., 2016, 2019; Rayagiri et al., 2018). Timely remodeling of the niche, a prerequisite for proper regeneration, is mediated by the controlled activation of different cell types including macrophages, eosinophils, neutrophils, fibro-adipogenic progenitors (FAPs), and fibroblasts (Dumont et al., 2015; Mashinchian et al., 2018; Murphy et al., 2011; Saclier et al., 2013; Theret et al., 2019). Aberrant signals from the MuSC niche caused, e.g., by chronic degenerative diseases leading to fibrosis, can impair MuSC function and regeneration (Serrano et al., 2011). During aging, the regenerative capacity of skeletal muscle declines, in part due to reduced numbers of MuSCs, but also due to reduced MuSC functionality. The impairment of MuSC function in the aged can be caused either by intrinsic changes in MuSCs or through changes in the stem cell niche, both resulting in impaired regeneration of skeletal muscle after injury (Brack and Muñoz-Cánoves, 2016; Chakkalakal et al., 2012; Ermolaeva et al., 2018; Lukjanenko et al., 2016; Rozo et al., 2016). Multiple MuSC-intrinsic signaling pathways have been identified to be aberrantly regulated in aged MuSCs, e.g., elevated JAK/STAT signaling (Price et al., 2014;

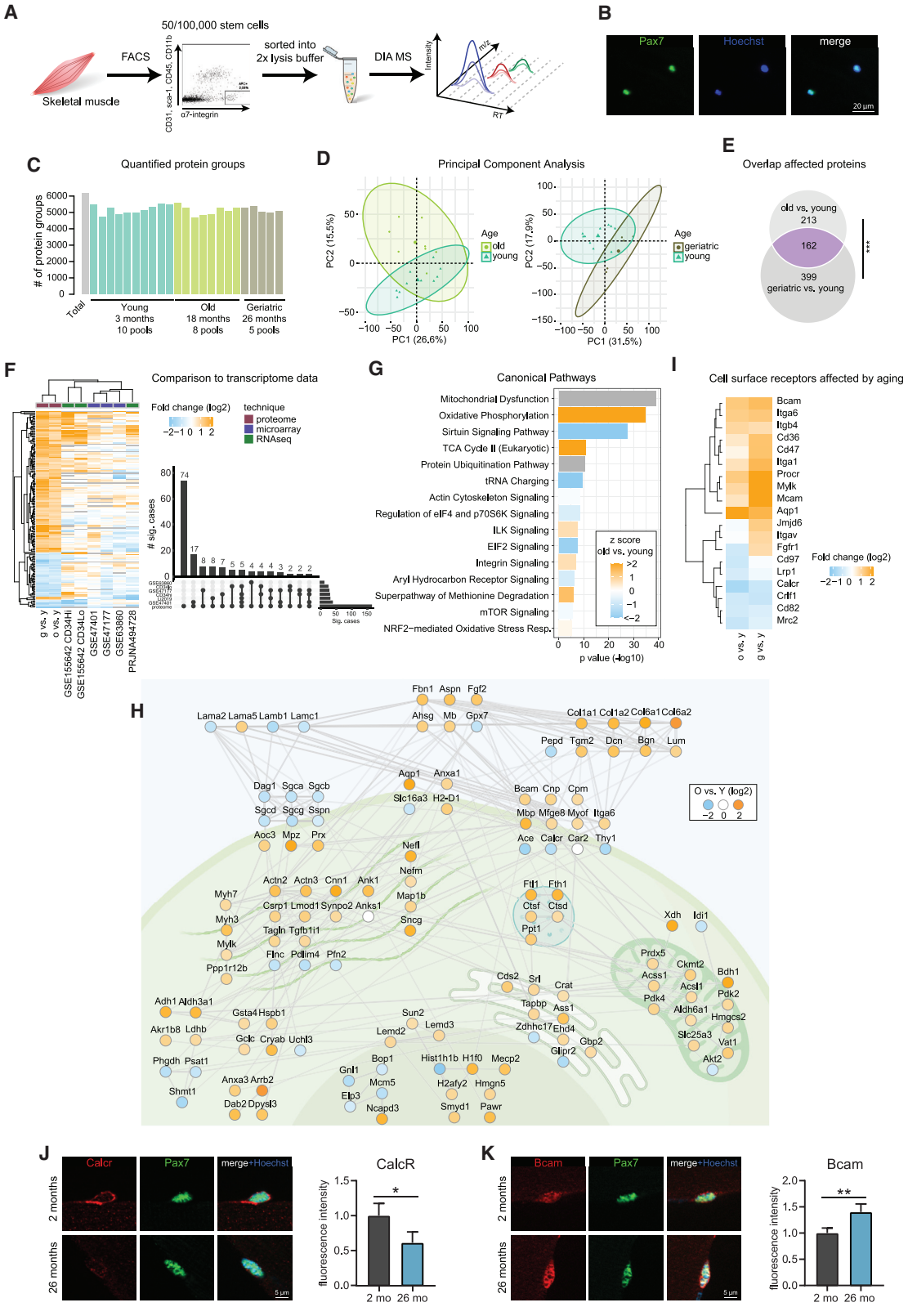

(legend on next page)

Tierney et al., 2014). Furthermore, increased senescence (Sousa-Victor et al., 2014) was shown to be caused by impaired autophagy in quiescent MuSCs from geriatric mice (García-Prat et al., 2016). In addition, MuSCs display perturbed Integrin beta-1 signaling during aging, which leads to aberrantly high ERK signaling upon stimulation. This then leads to a break of quiescence, ultimately resulting in depletion of the stem cell pool during aging (Rozo et al., 2016). Despite individual ECM proteins such as Fibronectin and Wisp1 having been shown to contribute to the functional impairment of MuSCs (Lukjanenko et al., 2016, 2019), a comprehensive characterization of the impact of aging on the MuSC niche is still missing, and consequently, the major signaling axes that connect extrinsic alterations to intrinsic changes in the aging MuSCs remain unclear.

Here, we investigate how aging alters the communication between MuSCs and their niche by studying in parallel the proteome of MuSCs and the composition of the skeletal muscle ECM during aging. We performed deep proteomic analyses of freshly isolated MuSCs and whole skeletal muscles across three different age groups ranging from young to geriatric mice. These data revealed MuSC-intrinsic changes in protein levels and an extensive remodeling of the MuSC niche during aging. Furthermore, we unraveled signaling axes potentially affected in MuSCs in relation to age-dependent changes in the MuSC niche. Among them, we identified the Integrin beta-1-mitogen-activated protein kinase (MAPK) signaling axis to be affected by the SPARC-related modular calcium-binding protein 2 (Smoc2), which accumulates in the MuSC niche during aging.

RESULTS

Aging changes the proteome of MuSCs

We first investigated which changes are occurring in MuSCs during aging. Therefore, we developed a proteomic workflow based on single-shot label-free data independent acquisition mass spectrometry that enabled us to study age-dependent changes of protein abundance in aging MuSCs (Figure 1A). Using freshly isolated MuSCs (Figure S1A–S1F; Pasut et al., 2012), we were able to reproducibly quantify over 4,500 proteins across 3 age groups (young: 3 months of age; old: 18 months of age; geriatric: 26 months of age), allowing us to investigate the progression of age-dependent changes (Figures 1B and 1C). This is especially important because the functionality of MuSCs is already impaired in old mice but further deteriorates in geriatric mice (Sousa-Victor et al., 2014). We compared 5–10 pools of MuSCs for each age group and revealed a distinct aging signature, as indicated by principal-component analysis (PCA) (Figure 1D) and differential expression analysis (Figure 1E and S1G; Table S1). Age-dependent transcriptome changes of MuSCs have been characterized in multiple studies; however, transcript levels can only partially predict changes at the protein level during aging due to a progressive decoupling between the transcriptome and proteome during aging (Janssens et al., 2015; Kelmer Sacramento et al., 2020; Ori et al., 2015; Wei et al., 2015). To investigate if the proteome and transcriptome are also uncoupled in aging MuSC, we re-analyzed transcriptome data from three independent studies based on microarray technology (Alonso-Martin et al., 2016; Liu et al., 2013; Lukjanenko et al., 2016; Price et al., 2014) and two recent datasets obtained by RNA sequencing (RNA-seq; García-Prat et al., 2020; Li et al., 2019). We compared age-related transcriptome and proteome changes by focusing on the 162 proteins significantly affected in both old and geriatric MuSCs (Figure 1E). Although proteome changes in old and geriatric MuSCs were highly correlated (Spearman rho = 0.8), we observed lower or no correlation with transcriptomics data, depending on the compared dataset (Spearman rho = 0 – 0.4) (Figure S1H). This analysis indicates that, also in MuSCs, a substantial proportion of age-dependent changes in protein abundance (74 out of 162, 45.7%) cannot be detected at the transcript level across multiple studies (Figure 1F). Calcitonin receptor (Calcr), Basal cell adhesion molecule (Bcam), SUN domain-containing protein2 (Sun2), and Integrin beta-4 (Itgb4) are examples of proteins being significantly changed in abundance during MuSC aging, although not all of them display consistent changes in transcript levels, a phenomenon that seems to be dependent also on the mRNA dataset

Figure 1. Proteomics analysis of MuSCs during aging

(A) Workflow showing isolation, processing, and mass spectrometric analysis of MuSCs.

(B) Immunofluorescence showing freshly isolated MuSCs stained for Pax7 (green) and Hoechst (blue). Scale bar: 20 μm.

(C) Number of quantified protein groups for each pooled MuSC sample from the three age groups (young: 3 months old, 10 pools analyzed; old: 18 months old, 8 pools analyzed; geriatric: 26 months old, 5 pools analyzed).

(D) PCA plots for old versus young and geriatric versus young MuSC samples. Ellipses represent 95% confidence intervals.

(E) Overlap of significantly affected proteins ($q < 0.05$ and absolute $\log_2$ fold change > 0.58) in old versus young and geriatric versus young comparisons. ***$p < 0.001$, Fisher's exact test.

(F) Comparison of aging MuSC proteomics data from this publication to aging MuSC microarray data from GSE63860, GSE47177, and GSE47401 and RNA-seq data obtained from PRJNA494728 and from CD34 high- and low-expressing MuSCs from GSE155642. The heatmap shows the comparison of protein and transcript fold changes. The upset plot shows the overlap of significant changes between proteome and transcriptome datasets. Proteins affected in both old and geriatric MuSCs (overlap shown in E) were used.

(G) Selected canonical pathways that are affected in old versus young MuSCs (Benjamini-Hochberg adjusted [adj.] $p < 0.01$). The color of each bar indicates the direction of regulation; orange increased and light blue decreased with aging. Gray color indicates pathways enriched among the age-affected proteins but for which a specific direction of regulation is not apparent.

(H) Network of aging-affected proteins in MuSCs. Interactions between proteins affected in both old and geriatric MuSCs were retrieved from String (Szklarczyk et al., 2019) (confidence score > 0.7). Only proteins displaying at least two interaction partners are shown.

(I) Cell surface receptors with known ligands (Ramilowski et al., 2015) affected by aging in either old or geriatric MuSCs.

(J and K) Immunofluorescence analysis of MuSCs on their adjacent myofibers directly fixed after isolation; Calcr (J) or Bcam (K) shown in red, Pax7 in green, and nuclei in blue. n > 20 MuSCs per mouse. Data are normalized to the average of the fluorescence intensities in young animals (set to 1). *$p < 0.05$; **$p < 0.01$; two sided, unpaired Student's t test. n = 4, 2 months and 26 months old. Error bars: SD. Scale bar: 5 μm. Related to Figures S1 and S2 and Table S1.

analyzed (Figure S2A–S2D). We confirmed that mRNA expression of Bcam, Sun2, and Itgb4 does not change significantly in aging MuSCs by using qRT-PCR analysis (Figure S2E–S2G).

Next, we wondered whether the identified proteome signature would recapitulate known aging pathways. Canonical pathway analysis identified mitochondrial dysfunction, decreased Sirtuin and eIF2 signaling, and a perturbation of the protein ubiquitination pathway, recapitulating alterations of metabolism and proteostasis that have been previously linked to the loss of MuSC functionality during aging (Kitajima et al., 2018; Ryall et al., 2015; Schüler et al., 2020; Zhang et al., 2016; Zismanov et al., 2016; Figures 1G and 1H; Table S1). Interestingly, we also identified a subset of pathways related to Integrin and Integrin-linked protein kinase (ILK) signaling (Figure 1G) and 19 cell surface receptors with known ligands to be affected in aging MuSCs (Ramilowski et al., 2015; Figure 1I), suggesting an altered communication with the stem cell niche. To verify the changes observed through mass spectrometry, we quantified the immunofluorescence signal for four candidate proteins in MuSCs on myofibers isolated from young and old mice. We observed a significant decrease in the abundance of Calcr (Figure 1J) in MuSCs from aged mice, whereas we observed significant increases in the abundance of Bcam and Sun2 as well as a trend for Itgb4 (Figure 1K; Figures S2H and S2I), validating our data obtained by mass spectrometry.

Aging progressively affects the proteome of skeletal muscle

Next, we asked which changes occur in the composition of the MuSC niche during aging. Therefore, we established a second proteomic strategy that allowed deep coverage (>4,000 protein groups in total) and reproducible quantification of the skeletal muscle proteome across the same three age groups used for MuSC analysis (Figures 2A and S3A). We analyzed four different muscles with different myofiber type composition, which relates to distinct metabolic properties (gastrocnemius, G; soleus, S; tibialis anterior, TA; extensor digitorum longus, EDL). To achieve maximum proteome coverage, tandem mass tag (TMT) analysis was performed. To be able to analyze five biological replicates per age group, we performed two TMT10plex experiments per muscle type and directly compared old versus young and geriatric versus young skeletal muscles. A clear impact of aging on the proteome of skeletal muscle was already detectable in old animals, as shown by PCA (Figures 2B and S3B). The direct comparison of proteins affected in different age groups revealed a subset of overlapping proteins, but also proteins that were exclusively altered in old or geriatric muscles, indicating the occurrence of different dynamics of age-dependent changes (Figure S3C). For three out of the four muscles investigated, we identified a higher number of differentially abundant proteins when comparing geriatric and young muscles than comparing old and young muscles, suggesting a progressive effect of aging on the skeletal muscle proteome (Figure 2C). In addition, the magnitude of fold changes was generally increased when geriatric muscles were compared to young muscles (Figure S3D), again supporting the notion that most age-dependent changes in the muscle proteome are progressive, and the extent and dynamics of proteome changes vary across the different muscles (Figures 2C and S3C; Table S2). Of note, PCA analysis of age-related protein fold changes showed a clear separation between the age comparisons (PC1, x axis), indicating a common proteome signature of aging independent of the muscles investigated (Figure 2D). Interestingly though, the PCA analysis also showed a separation by muscle type (PC2, y axis), with the soleus showing the most distinct aging signature in both age comparisons (Figure 2D).

Next, we performed a gene set enrichment analysis (GSEA) to identify pathways affected by aging. Thereby, we identified the following three major groups of pathways: (1) ECM, (2) mitochondria and energy metabolism, and (3) protein synthesis and mRNA splicing (Figure 2E; Table S2). These pathways were affected in all muscles that we analyzed; however, they showed distinct dynamics and, in some cases, opposite regulation between the different muscles (Figure S3E). We investigated in more detail rate-limiting enzymes for key metabolic pathways (Glycogen synthase 1 [Gys1], ATP-dependent 6-phosphofructokinase [Pfkm], Carnitine O-palmitoyltransferase 1 muscle isoform [Cpt1b], Isocitrate dehydrogenase [NADP] cytoplasmic [Idh1], Glucose-6-phosphate 1-dehydrogenase X [G6pdx], Fructose-1,6-bisphosphatase isozyme 2 [Fbp2]) and found muscle-specific aging signatures (Figure 2F). Furthermore, we observed an increase of respiratory chain proteins in TA, EDL, and gastrocnemius, whereas those proteins were decreased in the soleus during aging (Figures 2G and S3F). These findings are consistent with the known aging-dependent fiber type switch to a more oxidative fiber type (Larsson et al., 1993; Schiaffino and Reggiani, 2011). Finally, we found a decrease in the abundance of components of the protein synthesis machinery exclusively in the EDL (Figure 2H). Taken together, our data characterize the progressive effect of aging on the proteome of skeletal muscle and identify both common as well as muscle-type-specific changes in protein abundance.

Aging remodels the ECM in skeletal muscle and thereby the MuSC niche

Next, we investigated which cellular compartments are the most affected in skeletal muscle during aging (Figures 3A, 3B, and S4A). Consistent with GSEA (Figure 2E) and the known aging-dependent accumulation of ECM molecules (Lacraz et al., 2015), we observed a general increase in the abundance of extracellular or secreted proteins in geriatric muscles (Figures 3B and 3C; Figures S4B and S5A–S5E). Also for changes of ECM proteins, we observed an age-dependent clustering of the different muscles, with the soleus being separated from the fast twitched and mixed muscles (Figure S4C). Importantly, the composition of the ECM appears to be altered already in old animals for all the muscles analyzed, indicating that these alterations occur early in the aging process (Figure 3D; Figure S6A; Table S3). We further characterized those changes by focusing on the 421 proteins annotated as ECM/secreted according to Gene Ontology. A total of 183 of those 421 proteins were differentially abundant in at least 1 of the muscle types investigated at 18 months of age (Figure 3E). Although we identified some alterations in the abundance of ECM proteins that were muscle type specific (e.g., collagens; Figure S6B), the majority of changes in ECM proteins were shared by at least two of the muscle types

CellPress
OPEN ACCESS

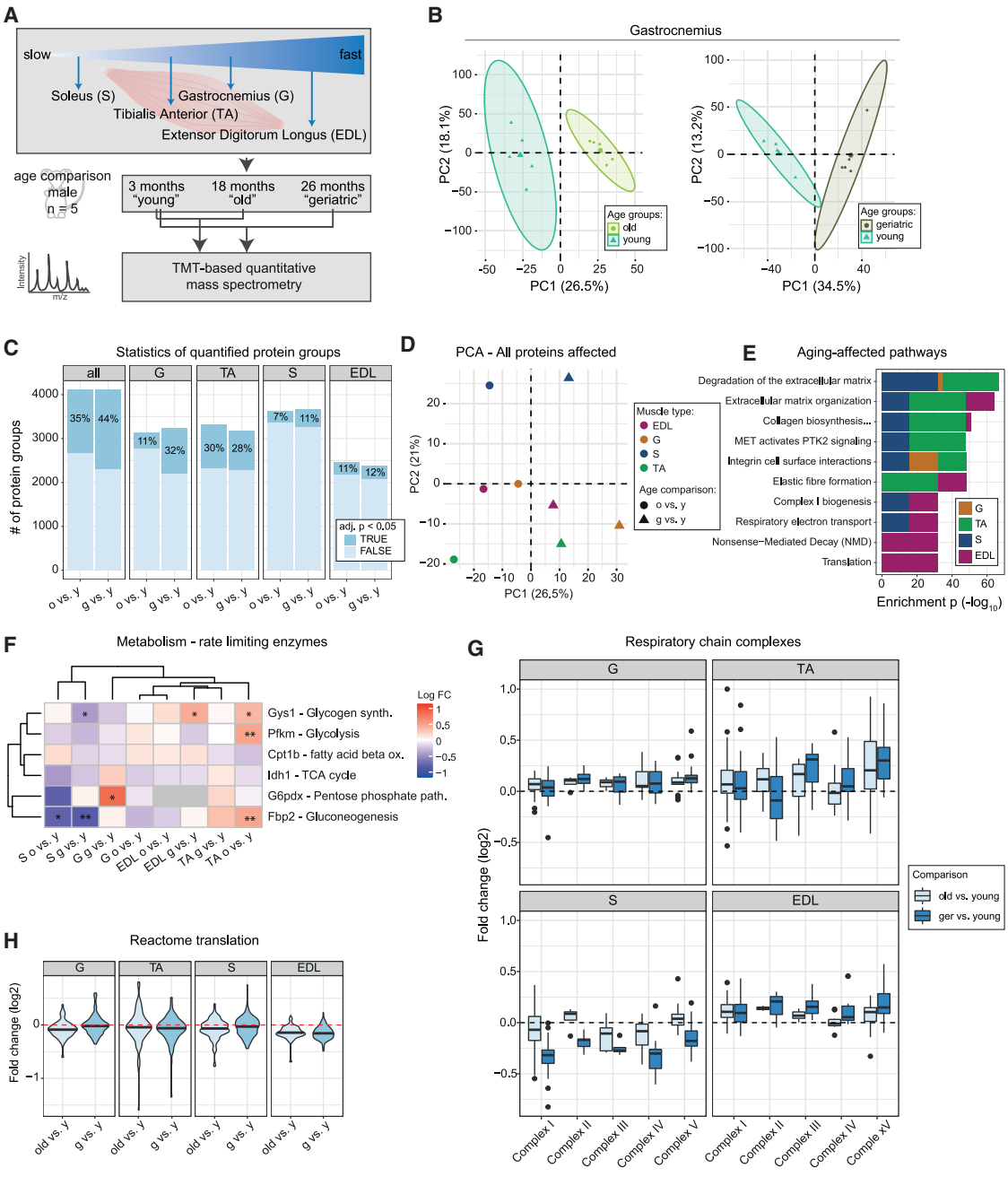

Figure 2. Age-dependent changes in the proteome of different skeletal muscles

(A) Schematic workflow of the proteomics experiment. Soleus (S), tibialis anterior (TA), gastrocnemius (G), and extensor digitorum longus (EDL) are shown in the order from slow to fast twitch muscles. For each muscle type, muscles from 18-month-old (old) and 26-month-old (geriatric) mice were compared to muscles from 3-month-old mice (young) in two separate TMT10plex experiments. n = 5 per sample group.

(B) PCA of young, old, and geriatric proteomics datasets from gastrocnemius. Ellipses represent 95% confidence intervals. The percentage of variance explained by each principal component is indicated.

(C) Number of quantified protein groups in each skeletal muscle analyzed and across all experiments. Significantly affected proteins (adj. $p < 0.05$) are indicated in dark blue.

(D) PCA plot of age-related proteome changes in different muscle types. The percentage of variance explained by each principal component is indicated.

(E) GSEA showing 10 of the most affected pathways during skeletal muscle aging using WebGestalt (Liao et al., 2019).

(F) Heatmap showing fold changes of rate limiting enzymes of different metabolic pathways. **$q < 0.01$, *$q < 0.05$.

(G) Age-related fold changes of proteins belonging to the different respiratory chain complexes.

(H) Violin plots showing log2 fold changes of proteins related to translation across all muscles and age comparisons. Related to Figures S3 and S4 and Table S2.

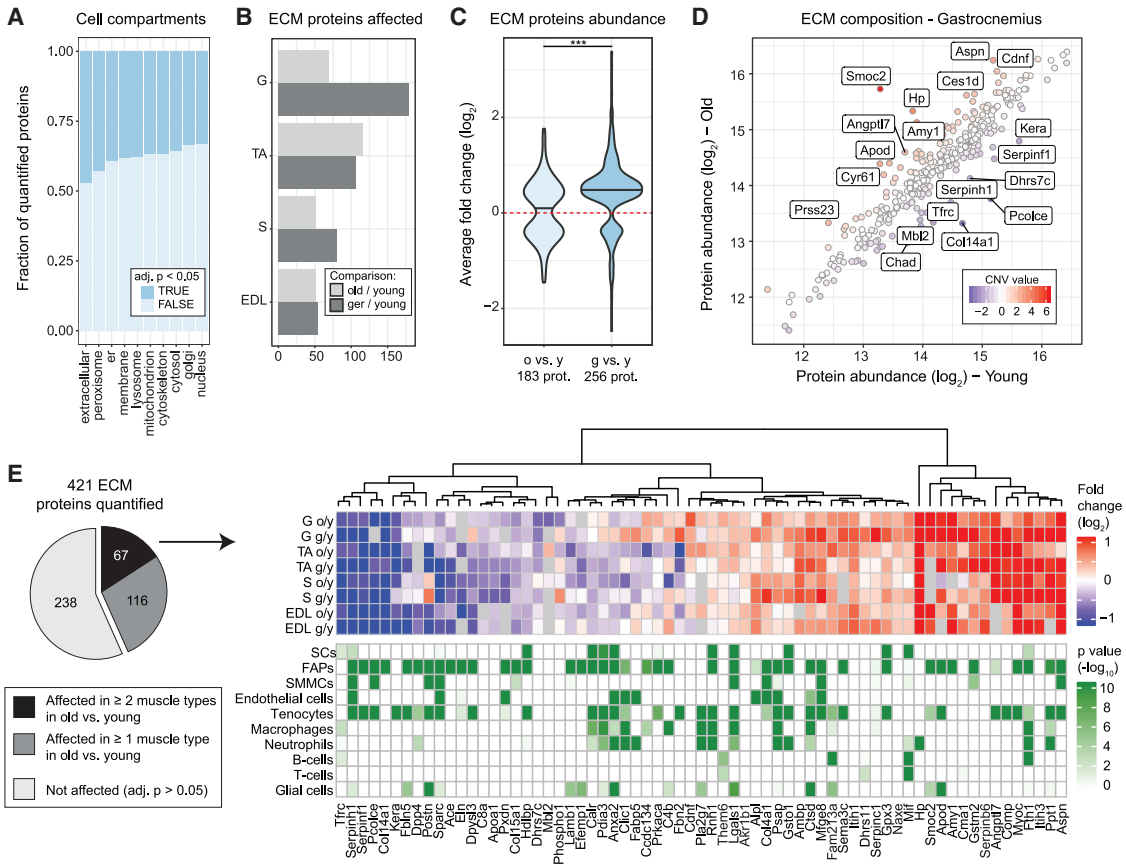

Figure 3. Remodeling of the MuSC niche during aging

(A) Fraction of significantly affected proteins (adj. p < 0.05) across all muscles and age comparisons analyzed for the different cellular compartments.

(B) Bar plot showing the number of significantly affected ECM proteins across different muscles.

(C) Violin plot showing average log2 fold changes for all significantly affected ECM proteins quantified across muscles (***p < 0.001, Wilcoxon rank-sum test with continuity correction).

(D) Scatterplot comparing the abundance of ECM proteins in young (x axis) and old (y axis) gastrocnemius. The red-blue color code indicates for each protein the residual value of the linear model fitted on all the ECM proteins quantified (compartment normalized value, CNV; Parca et al., 2018).

(E) ECM proteins affected by aging, classified according to being significantly affected (adj. p < 0.05). Fold changes for the 67 ECM proteins affected in at least 2 different muscles are shown as a heatmap (top). The expression of the same proteins across cell types of skeletal muscle is shown (bottom heatmap). Single-cell expression data were obtained from Giordani et al. (2019). The shade of green indicates the p value for the enrichment of cells expressing transcripts as determined by a hypergeometric test. SCs, satellite cells; FAPs, fibro-adipogenic-progenitors; SMMCs, smooth muscle and mesenchymal cells. Related to Figures S4, S5, and S6 and Table S3.

investigated (Figure S6C). Therefore, we focused our further analyses on the 67 proteins that showed consistent age-dependent changes across different muscles at an age of 18 months. Of note, the vast majority of significantly affected proteins showed a consistent increase or decrease of abundance with aging across all four muscles investigated (Figure 3E).

To investigate which cell types contribute the most to the remodeling of the MuSC niche during aging, we integrated single-cell RNA-seq data from adult skeletal muscle (Giordani et al., 2019) with our proteome data. To identify the cell type(s) expressing the identified ECM proteins affected by aging, we used a hypergeometric test, as implemented in scfind (Lee et al., 2019; see STAR Methods for details). Thereby, we mapped the majority of ECM proteins changed in aging skeletal muscle to at least one cell type (53/67, 79%; Figure S6D). We found FAPs to predominantly express transcripts for ECM proteins affected by aging (42/67, 63%), indicating that cells of mesenchymal origin are the major contributors to the aging-dependent remodeling of the ECM in skeletal muscle (Figures 3E and S6E). Taken together, we identified an aging signature of the ECM that is conserved between different skeletal muscles, supporting the notion that the MuSC niche is progressively remodeled with increasing age independent of the fiber type composition of the muscle.

Aging perturbs the communication axes between MuSCs and their niche

In order to identify the main axes of communication between MuSCs and their niche that are perturbed during aging, we used known ligand-receptor interactions (Ramilowski et al., 2015). In brief, the identification of receptors that are expressed

CellPress
OPEN ACCESS

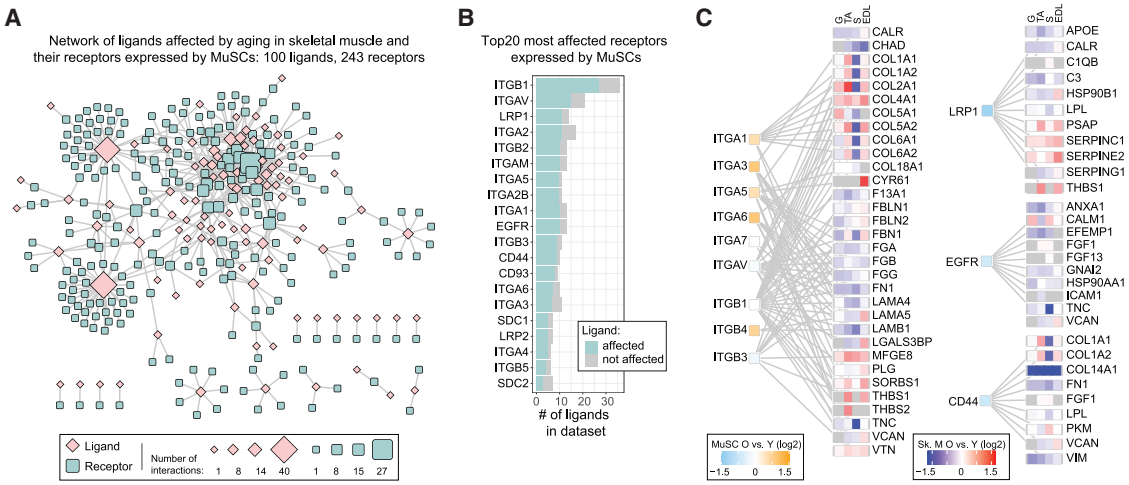

Figure 4. Network analysis of changes in the MuSC niche and receptors in MuSC during aging

(A) Network derived from 100 ligands with known receptors (Ramilowski et al., 2015) that were significantly changed in at least 1 of the skeletal muscle aging comparisons, and 243 receptors expressed by MuSCs according to GEO: GSE63860, GSE47177, and GSE81096.

(B) Top 20 affected receptors in MuSCs, ranked by the number of ligands that change in abundance during aging. Displayed are the total number of quantified ligands in the skeletal muscle aging proteomics dataset of this study (gray) and the number of significantly changed proteins (green, adj. $p < 0.05$).

(C) Heatmap showing the protein fold changes of selected receptors from (B) that were quantified in the MuSC proteomics dataset and the connection to their ligands that were significantly altered in their abundance in the aging skeletal muscles. Related to Figure S7 and Table S4.

by MuSCs was based on detectable mRNA levels in different datasets, whereas the analysis of which receptor-ligand axes are mainly affected during aging was based on the proteomics data generated here. Thereby, we connected ECM/secreted proteins that we found to be affected in at least one muscle type at old age with cell surface receptors that are expressed by MuSCs (Alonso-Martin et al., 2016; Liu et al., 2013; Lukjanenko et al., 2016; Price et al., 2014; Table S4). This network analysis revealed the existence of clusters of receptors in MuSCs that displayed multiple interactions to be affected by changes in ligand abundance in the old MuSC niche (Figure 4A; Figure S7A). Through ranking the receptors expressed by MuSCs based on the number of predicted affected interactions, we revealed multiple Integrin-related cell surface proteins, Lrp1, Egfr, and Cd44, as the main receptors for ECM/secreted proteins affected through aging in the MuSC niche (Figures 4B and 4C). Interestingly, the abundance of all of those receptors was also directly changed in MuSCs in an age-dependent manner. The abundance of Integrin-related proteins was generally increased, whereas Egfr and Cd44 showed decreased abundance in aged MuSCs (Figure 4C). These results, together with the findings that (1) Integrin signaling is an affected aging pathway in MuSCs (Figures 4B and 4C), (2) Integrin beta-1 was shown to display abnormal localization in aged MuSCs causing altered activation (Rozo et al., 2016), and (3) Egfr is a predicted major upstream regulator of intrinsic changes in our MuSC proteome dataset (Figure S7B; Table S1), underline the interconnectivity between changes in the MuSC niche and intrinsic alterations during MuSC aging.

The abundance of the ECM protein Smoc2 increases during aging and upon injury in the MuSC niche

Because regeneration is severely impaired during aging and it is known that changes in the ECM directly affect functionality of MuSCs (Baghdadi et al., 2018; Bentzinger et al., 2013b; Lukjanenko et al., 2016; Rayagiri et al., 2018), we searched for ECM proteins that show differential abundance during aging under homeostatic conditions and during regeneration in the young. Therefore, we generated a proteomic dataset of young regenerating TA muscles at day 7 after CTX (cardiotoxin) injury and analyzed the changes in abundance of the 67 ECM proteins affected during aging in resting skeletal muscle (Table S5). We found that the majority of ECM proteins displaying age-dependent changes in abundance also showed changes during regeneration (57 of the 65 proteins quantified in both datasets, 88%; Figure 5A). We chose Smoc2, Asporin, Elastin, and Collagen alpha-1(XIV) chain (Col14a1) for further validation because (1) they are among the most prominently affected proteins in skeletal muscle during aging (Figures S5A–S5E, 5F–5K, S8O, and S8P), (2) their levels progressively increase or decrease with age (Figures S8A–S8N), and (3) their abundance is increased during regeneration (Figures 5B–5E).

We focused on Smoc2 for further investigations and found *Smoc2* mRNAs to be primarily expressed in FAPs and tenocytes (Figure 5L). We confirmed that *Smoc2* remains primarily expressed by mesenchymal cells at old age by analyzing the Tabula muris senis single-cell RNA-seq dataset (Pisco et al., 2019; Figure S9A). To verify that *Smoc2* is transcribed by FAPs in skeletal muscle, we performed qRT-PCR on freshly isolated FAPs from young and old mice and on primary myoblasts isolated from young mice. Indeed, *Smoc2* transcript levels were significantly higher in freshly isolated FAPs from both young and old mice than those in primary myoblasts, further supporting the notion that FAPs are the primary source of Smoc2 in skeletal muscle (Figure 5M). The secretion of Smoc2 protein by FAPs was demonstrated by targeted proteomic analysis of conditioned media from cultured FAPs (Figures 5N and S9B) and

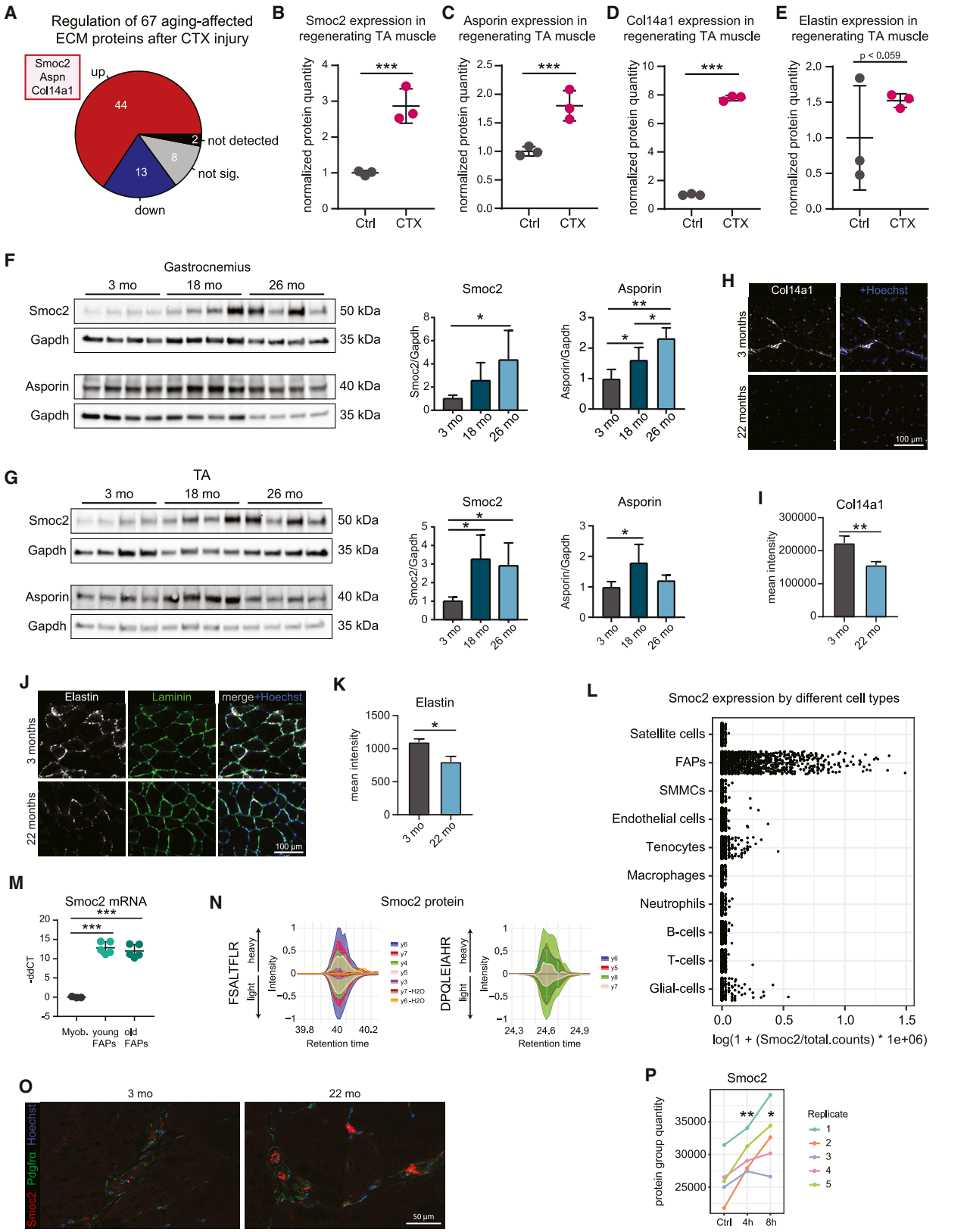

(legend on next page)

co-immunofluorescence staining of Smoc2 and Pdgfrα, a marker for FAPs (Figure 5O). Of note, Smoc2 accumulated in cultured FAPs after Monensin treatment, further strengthening our finding that FAPs are the main cells secreting Smoc2 in skeletal muscle (Figure 5P).

FAPs from young and old mice appeared to express similar levels of *Smoc2* transcript (Figure 5M). Consistently, no age-dependent increase in transcript levels was observed for *Smoc2* in bulk RNA-seq from whole skeletal muscle (Figure S9C). These data suggest that the increased levels of Smoc2 protein in old muscles derive from an accumulation of the protein in the ECM rather than from increased transcription. To test this hypothesis, we decellularized TA muscles from young and old mice and analyzed them by quantitative mass spectrometry (Table S6). Efficient decellularization was confirmed by a significant decrease in the DNA-to-tissue weight ratio compared to that of native tissue at both ages (Figure S9D). Indeed, we found Smoc2 to be among the proteins with the largest increase in decellularized old TA muscles, confirming its accumulation in the ECM during aging (Figure S9E).

Smoc2 contributes to perturbed Itgb1-dependent signaling in MuSCs during aging

Next, we hypothesized that aberrantly high levels of Smoc2 might contribute to altered Integrin signaling in MuSCs because Smoc2 was previously shown to stimulate signaling via ILK (Liu et al., 2008). First, we confirmed the interaction between Smoc2 and components of Integrin signaling complexes by affinity purification followed by quantitative mass spectrometry by using a cell line expressing Smoc2 fused to GFP (Figure S10A). After validating the expression of Smoc2-GFP and GFP control (Figures S10B and S10C), we focused our analysis on cell surface proteins and searched for proteins exclusively identified in eluates from Smoc2-GFP-expressing cells. Among those proteins, we identified Integrin beta-1 (Itgb1) as an interaction partner of Smoc2 (Figure 6A). Interestingly, we also found ILK to be bound to Smoc2-GFP complexes, further supporting the interaction between Smoc2 and components of the Integrin signaling pathway (Figure 6A). Through a proximity ligation assay (PLA), we demonstrated a close proximity of Smoc2 and Itgb1 in MuSCs in floating myofiber culture, indicating that Smoc2 and Itgb1 interact also in MuSCs (Figure 6B).

Next, we tested activation of Itgb1-dependent signaling by Smoc2 in myogenic cells. We found a mild, but significant, increase of pERK 10 min after addition of the Smoc2 recombinant protein in myogenic cells. This was followed by a reduction of pERK levels 60 min after addition of Smoc2, which is consistent with the described transient activation of MAPK signaling by different activators in cell culture (Cirit et al., 2012; Kiyatkin et al., 2006; Pronsato et al., 2012; Figures 6C and S10D). We confirmed the activation of pERK signaling by Smoc2 by using phospho-proteomics analysis. In particular, we found known targets of pERK, such as Tnks1bp1 (S763) (Courcelles et al., 2013), and ERK1/2 itself (Y185) to display increased phosphorylation upon addition of Smoc2 (Figures 6D and S10E; Table S7). Of note, phosphorylation of Itgb1 at T777 was also increased upon Smoc2 supplementation, supporting the notion that Smoc2 signals via the Itgb1/ERK axis (Figure 6D).

Next, we tested if addition of the Smoc2 recombinant protein is sufficient to activate transcription of MAPK target genes in young MuSCs by using the floating myofiber culture system. This method allows the investigation of MuSCs in their endogenous niche in an otherwise defined environment (Hüttner et al., 2019; Pasut et al., 2012). We found that addition of the Smoc2 recombinant protein is sufficient to increase the expression of target genes downstream of the MAPK signaling pathway (i.e., p57 and Ets2), whereas target genes of other signaling pathways known to be important for MuSC functionality in general and of which some are also altered in MuSCs during aging were not affected (canonical Wnt, Smad, Notch, and JAK/STAT pathways; Figure 6E; Figure S10F; Brack et al., 2007; Chakkalakal and Brack, 2012; Price et al., 2014; Rozo et al., 2016). To demonstrate that induction of ERK phosphorylation through Smoc2 is dependent on Itgb1, we transfected MuSCs on isolated myofibers with small interfering RNA (siRNA) directed against Itgb1 (siItgb1) or a non-targeting

Figure 5. Validation of proteomics data and demonstration that Smoc2 is mainly expressed and secreted by FAPs

(A) Pie chart showing the 67 ECM proteins identified in Figure 3E and how they are regulated 7 days after CTX injury in TA muscle. n = 3, 3 months old.

(B–E) Mass spectrometry analysis of Smoc2 (B), Asporin (C), Col14a1 (D), and Elastin (E) expression 7 days after CTX injury. Normalized protein quantity is displayed, normalized to the uninjured control. n = 3, 3 months. *** adj. $p < 0.001$.

(F and G) Immunoblot analysis of gastrocnemius (F) and TA (G) homogenates for Smoc2 (Isoform 1), Asporin, and Gapdh with quantification of Smoc2 and Asporin levels relative to Gapdh. n = 4 per group, age: 3 months, 18 months, 26 months. *$p < 0.05$; one-way ANOVA.

(H) Representative images of immunofluorescence stainings of Col14a1 (white) with Hoechst (blue) in TA muscles of 3 months and 22 months old mice. Scale bar: 100 μm.

(I) Quantification of (H). **$p < 0.01$; n = 4 per group, age: 3 months, 22 months; two sided, paired Student's t test.

(J) Representative images of immunofluorescence analysis of Elastin (white) with Laminin (green) and Hoechst (blue) in TA muscles of 3-month-old and 22-month-old mice. Scale bar: 100 μm.

(K) Quantification of (J). *$p < 0.05$; n = 4, 3 months and n = 3, 22 months; two-sided, paired Student's t test.

(L) Bar plot showing the expression levels of Smoc2 based on single-cell transcriptomics data from Giordani et al. (2019).

(M) Transcript levels of Smoc2 on sorted FAPs (n = 5, 2-month-old mice) and myoblasts (n = 3), normalized to the average delta cycle threshold (dCT) of myoblast samples. ***$p < 0.001$; one-way ANOVA.

(N) Detection of Smoc2 peptides in conditioned media of cultured FAPs by parallel reaction monitoring using heavy spike-in peptides FSALTFLR and DPQLEIAHR. For additional replicates, see Figure S9B.

(O) Representative images of immunofluorescence staining for Smoc2 (red), Pdgfrα (green), and Hoechst (blue) of TA sections from 3-month-old and 22-month-old mice. Scale bar: 50 μm.

(P) Smoc2 protein abundance in cultured FAPs after inhibition of secretion by Monensin (4 h and 8 h). **$p < 0.01$, *$p < 0.05$; two-sided, paired Student's t test compared to Ctrl. Error bars: SD. Related to Figures S8 and S9 and Table S5.

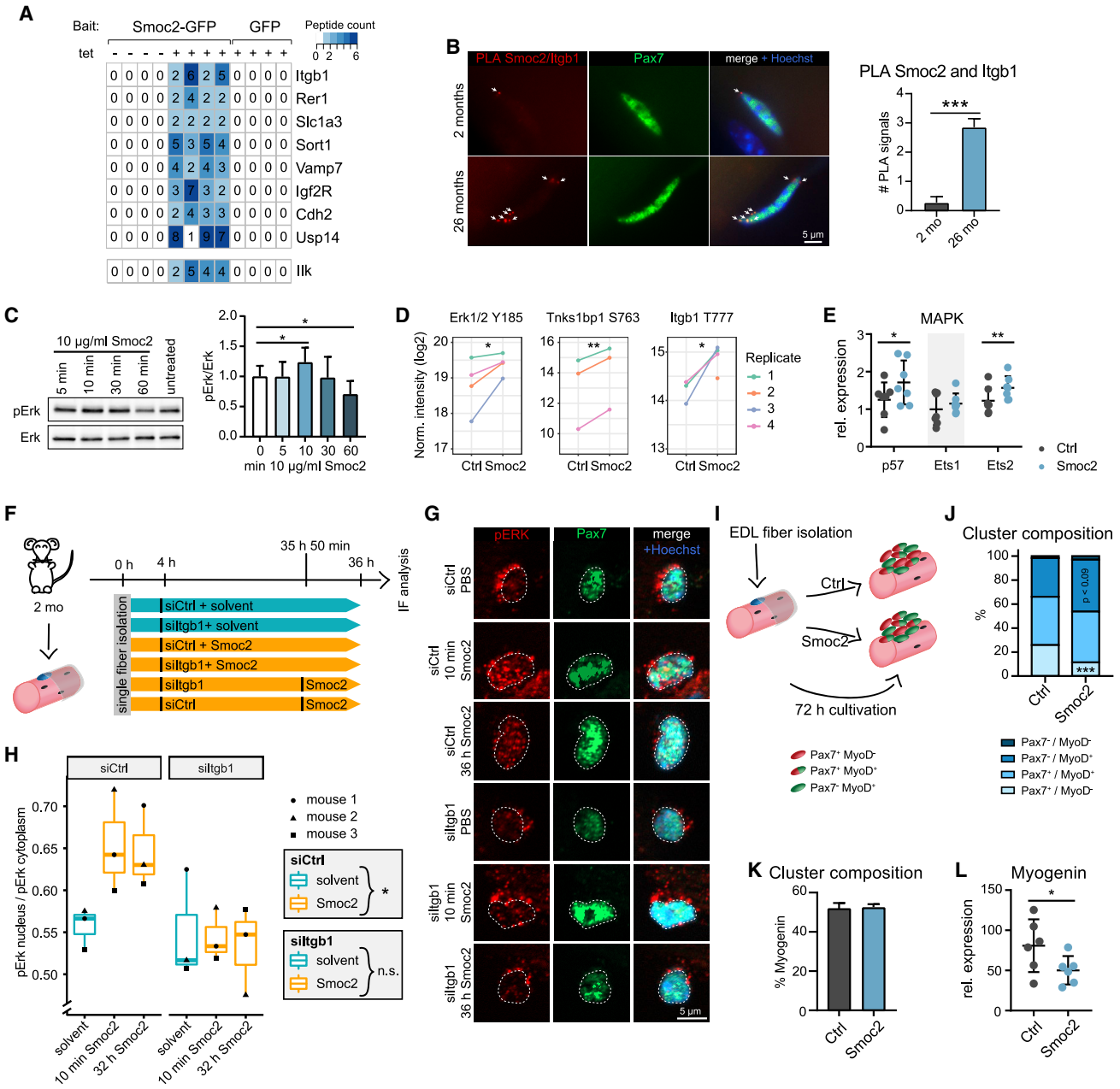

Figure 6. Smoc2 interacts with Integrin beta-1, induces activation of the ERK pathway, and affects MuSC behavior

(A) Cell surface proteins identified as potential interaction partners of Smoc2. Peptide counts for all proteins annotated to the cell surface Gene Ontology (GO) term (GO: 0009986) enriched in eluates from Smoc2-GFP expressing cells. n = 4.

(B) Proximity ligation assay (PLA; shown in red and marked by arrows) using antibodies directed against Smoc2 and Itgb1 on MuSCs in floating myofiber culture of 2-month-old and 26-month-old mice. Number of PLA signals per Pax7-positive cell (in green) was quantified. ***$p < 0.001$; two-sided, unpaired Student's t test. n = 5. Scale bar: 5 µm.

(C) Immunoblot analysis of pERK and ERK in C2C12 cells at different time points after 10 µg/ml Smoc2 treatment. pERK levels were normalized to ERK levels. *$p < 0.05$; two-sided, paired Student's t test. n = 3.

(D) Phospho-proteome analysis of C2C12 cells at different time points after 10 µg/ml Smoc2 treatment. Normalized phosphosite intensities are shown for Erk1/2 Y185, Tnks1bp S763, and Itgb1 T777. **$p < 0.01$, *$p < 0.05$. n = 4.

(E) qPCR analysis of different MAPK downstream targets in MuSCs on floating myofibers after Smoc2 treatment. Values are normalized to the expression level at 0 h after isolation (set to 1), **$p < 0.01$, *$p < 0.05$; two-sided, paired Student's t test. n = 7, 2-month-old mice, 5 µg/ml Smoc2 treatment at 0 h and 32 h after isolation.

(F) Schematic showing the experimental setup; 10 µg/ml Smoc2 were used for either 32 h or 10 min.

(G) Representative images for (F) showing pERK (red), Pax7 (green), and Hoechst (blue). Scale bar: 5 µm.

(legend continued on next page)

control siRNA (siCtrl), incubated them with either Smoc2 or a solvent control, and quantified pERK staining intensity in the nucleus in relation to the total pERK signal in the same cell (Figures 6F–6H). Thereby, we could show that phosphorylation of ERK following administration of Smoc2 is dependent on Itgb1. Of note, even a short incubation with Smoc2 recombinant protein (10 min) was sufficient to induce phosphorylation and shuttling of ERK into the nucleus (Figures 6F–6H).

To further assess the functional consequences of aberrantly increased levels of Smoc2 on MuSCs, we cultured young MuSCs on their adjacent myofibers with and without the recombinant Smoc2 protein for 72 h, a time point when clusters of MuSCs have formed comprising self-renewing MuSCs, committed MuSCs, and differentiated cells such as myoblasts (Schmidt et al., 2019; Figure 6I). We quantified the percentage of Pax7+/MyoD− self-renewing, Pax7+/MyoD+ committed, and Pax7−/MyoD+ differentiated cells per cluster after 72 h of culture and found that addition of Smoc2 recombinant protein reduced the ability of MuSCs to self-renew (Pax7+/MyoD− cells), whereas early differentiation (Pax7−/MyoD+ cells) was not impaired, which is a phenotype reminiscent of aged MuSCs (Figures 6J and S10G; Price et al., 2014). Interestingly, the number of clusters per myofiber and the cluster size were not affected, suggesting that Smoc2 does not impair activation or proliferation of MuSCs per se but rather their self-renewal (Figures S10H and S10I). We then asked whether or not addition of Smoc2 recombinant protein affects terminal differentiation of MuSCs. Therefore, we analyzed the number of myogenin-positive cells per cluster and expression of *myogenin* mRNA, a marker for terminal differentiation, after supplementing the myofiber cultures with recombinant Smoc2 protein. When analyzing the percentage of myogenin+ cells per cluster, we did not observe differences in the percentage of myogenin-positive cells per cluster (Figure 6K). However, addition of Smoc2 recombinant protein reduced the expression of *myogenin* mRNA, whereas total *Pax7* mRNA levels showed a slight, but not significant decrease, and total *MyoD* mRNA expression did not change (Figures 6L and S10J). Taken together, these data suggest that elevated Smoc2 levels—as found in the aged MuSC niche—activate MAPK signaling in MuSCs through Itgb1 and impair their functionality.

Exogenous Smoc2 protein mildly affects muscle regeneration upon repeated injury

Regeneration of skeletal muscle is accompanied by dynamic remodeling of the MuSC niche to promote each step of the regeneration process in a specific manner (Schmidt et al., 2019; Wosczyna and Rando, 2018). To identify at which step Smoc2 is most likely affecting the regeneration process, we investigated the dynamics of Smoc2 expression during regeneration after CTX-induced injury in young mice. We found that Smoc2 protein levels display two peaks of expression, namely, at day 2 after injury as well as at day 4/5 after injury, which are the time points of MuSC activation and proliferation (Bentzinger et al., 2013a), suggesting that Smoc2 might directly affect MuSC behavior during early regeneration (Figures 7A and S10K). To estimate the total amount of Smoc2 in a TA muscle, we performed absolute protein quantification by using targeted proteomic analysis based on spike-in reference peptides. Thereby, we estimated an endogenous concentration of 0.33 fmol Smoc2 per μg total protein in 18-month-old mice, resulting in approximately 115 ng of Smoc2 per TA muscle (Figure 7B).

Next, we injured the TA muscle of 3-month-old mice with CTX, followed by injection of Smoc2 (10 μg recombinant protein, ~87× relative to endogenous concentration) or a control at day 3 and 5 after injury (Figure 7C). Unexpectedly, we did not observe an impairment of the regeneration process at day 10 of regeneration after a single injury (Figures 7D and 7E). The percentage of newly formed myofibers, marked by the expression of developmental myosin heavy chain (devMHC), as well as the myofiber size, was not significantly different under Smoc2 versus control conditions (Figures 7D and 7E). Accordingly, the amount of Pax7+ MuSCs per myofiber was not altered (Figures 7F and 7G). Concomitantly, no obvious alterations in Sirius red staining, a marker for fibrotic tissue, were observed following injection of the Smoc2 recombinant protein (Figure S10L). Therefore, we investigated how aberrant protein amounts of Smoc2 affect regeneration and MuSC numbers in a setting of constant regeneration. Thus, we performed a serial injury experiment in young mice, as follows: the same TA muscle was injured 3 times every 14 days, and Smoc2 recombinant protein or a control was injected at day 3 and 5 following each round of injury. Thereby, we created a condition in which MuSCs are constantly challenged and dividing. Muscles were harvested and analyzed 21 days after the last injury, which is a time point at which most MuSCs have stopped dividing and the regeneration process is nearly complete (Rogers et al., 2015; Figure 7H). Under these conditions, we observed that regeneration of skeletal muscles injected with the Smoc2 recombinant protein was perturbed, as evidenced by an increased percentage of devMHC-positive myofibers and smaller myofiber sizes in the Smoc2-injected muscles (Figures 7I–7K). Interestingly, addition of Smoc2 recombinant protein only slightly reduced the number of MuSCs per myofiber (Figures 7L and 7M). Similar to the data observed after a single injury, we did not observe an

(H) Quantification of nuclear pERK to total pERK. n > 20 cells per mouse and condition. *p < 0.05, two-way ANOVA. n = 3, 2-month-old mice.
(I) Schematic showing the floating myofiber culture assay.
(J) Analysis of the number of Pax7- and MyoD-expressing cells in clusters on floating myofibers. Displayed values are the percentage of cells in a cluster expressing neither Pax7 nor MyoD (Pax7−/MyoD−), Pax7 only (Pax7+/MyoD−), MyoD only (Pax7−/MyoD+), or both (Pax7+/MyoD+). ***p < 0.001; two-sided, paired Student's t test. n = 4, 3-month-old mice, 5 μg/ml Smoc2.
(K) Analysis of the number of myogenin-positive cells per cluster using the floating myofiber culture system. Displayed values are the percentage of cells in a cluster expressing myogenin. n = 4, 2-month-old mice, 5 μg/ml Smoc2 treatment at 0 h and 42 h after isolation.
(L) qPCR analysis for myogenin in MuSCs on floating myofibers. Expression levels are indicated relative to levels of directly processed samples (0-h cultivation set to 1). **p < 0.01, *p < 0.05; two-sided, paired Student's t test. n = 6, 2-month-old mice, 5 μg/ml Smoc2 treatment at 0 h and 32 h after isolation. Error bars: SD.
Related to Figure S10 and Table S7.

obvious increase in fibrosis following injection of the Smoc2 recombinant protein (Figure S10M). We suggest that the aberrant levels of Smoc2 during aging are a contributing, but not exclusive, factor that transiently impair MuSC functionality and skeletal muscle regeneration in the aged.

DISCUSSION

Here, we established two distinct proteomics approaches that enabled us to analyze the proteome of MuSCs and whole skeletal muscle during aging. With these workflows, we were able to establish a connection between intrinsic changes in MuSCs and changes in the skeletal muscle niche, particularly of the ECM. Furthermore, the combined approach allowed us to identify candidate signaling axes that link impaired MuSC functionality during aging to age-dependent changes in the ECM.

The integration of our proteomics data from MuSCs and skeletal muscles showed that several ECM proteins affected by aging converge on a few major axes of inter-cellular communication, including Integrin signaling, corroborating previous findings that demonstrated dysfunctional Itgb1 signaling in aging MuSCs (Rozo et al., 2016). Our data reveal the complexity of signaling rewiring in the aged skeletal muscle mediated by changes in the abundance of multiple ligands in the MuSC niche and by changes in cell surface receptors on MuSCs (e.g., decreased levels of Calcr and increased levels of Itgb4). Our analyses indicate that FAPs are the primary cell of origin for the majority of ECM proteins showing age-dependent differences. Because the numbers of FAPs do not increase with age (Lukjanenko et al., 2019), we speculate that gene expression programs of FAPs change during aging, leading to an altered abundance of specific ECM molecules. For instance, it was recently shown that the ECM molecule Wisp1 is severely reduced in the aged ECM of skeletal muscle and that this decrease is due to changes in aged FAPs (Lukjanenko et al., 2019). Additional mechanisms independent of transcriptional changes, e.g., altered protein turnover due to decreased degradation or increased protein synthesis and secretion, could also lead to the accumulation of proteins in the ECM of aged skeletal muscle, as it appears to be the case for Smoc2. Finally, the contribution of other cell types to the ECM remodeling should not be underestimated because a considerable fraction of aging-affected ECM proteins originates from other cell types, including immune cells, fibroblasts, and MuSCs themselves.

In different cell types, a decoupling of the proteome from the transcriptome has been observed during aging (Janssens et al., 2015; Kelmer Sacramento et al., 2020; Ori et al., 2015; Wei et al., 2015). We identified a similar decoupling in MuSCs, which involves half of the proteins that we detected as affected by aging. We propose that decoupling of the transcriptome and proteome in MuSCs is at least partially caused by posttranscriptional mechanisms regulating protein abundance, including altered protein degradation by the lysosome-autophagy and ubiquitin-proteasome systems, as observed in other aging tissues such as the brain, muscle, and heart (Bulteau et al., 2002; Ferrington et al., 2005; Kelmer Sacramento et al., 2020; Schüler et al., 2020) and changes in protein synthesis rates. Consistent with our observations, a decreased proteolytic activity by the lysosome-autophagy system has been described in aging MuSCs (García-Prat et al., 2016). Furthermore, proteasome function has been shown to be required for the maintenance of the MuSC pool (Kitajima et al., 2018), whereas altered control of protein synthesis by mutation of eIF2 alpha leads to spurious activation of MuSCs and reduces the muscle regenerative capacity (Zismanov et al., 2016). However, we observed a substantial heterogeneity between different transcriptomic studies, at least for the group of genes investigated in this study. A similar heterogeneity has also been described for transcriptomic datasets of aging hematopoietic stem cells (Svendsen et al., 2020). Thus, we cannot exclude that differences in sample preparation, sorting strategies, and age groups used in the different studies (Table S1) might—at least in part—account for the observed differences between the proteome and transcriptome data. Our findings emphasize the necessity of having a dedicated workflow to also detect alterations that are only observable on the protein level and, subsequently, lead to functional changes during aging. With the proteomic workflow presented here, a combined analysis of the bulk proteome and transcriptome of MuSCs will be possible in the future, enabling a deeper understanding of functional changes during aging.

We identified Smoc2 as a player that contributes to altered Integrin signaling in MuSCs during aging. We have shown that increased levels of Smoc2 result in the activation of MAPK/ERK1/2 signaling by Itgb1 in myogenic cells. Signaling downstream of Itgb1 connecting changes in the ECM to changes in the MuSCs themselves has been shown to be perturbed in aging MuSCs, resulting in impaired MAPK signaling (Lukjanenko et al., 2016; Rozo et al., 2016). We suggest that Smoc2 is one of the ECM factors contributing to alterations of Itgb1 activity in aged MuSCs, although we cannot exclude the involvement of other receptors/signaling pathways. Because Smoc2 was previously shown to promote cell cycle progression in several cell types (Liu et al., 2008; Rocnik et al., 2006; Su et al., 2016), we hypothesize that Smoc2 is preventing the return of MuSCs to quiescence following activation, presumably by ERK signaling. This is in line with data from Rozo et al. (2016) demonstrating that ERK signaling is the most activated signaling pathway in MuSCs downstream of Itgb1, whereas activation of AKT is rather mild (Rozo et al., 2016). Chronic exposure to elevated Smoc2 levels might lead to stem cell exhaustion during aging and upon repeated injury. Indeed, we could show that elevated levels of Smoc2 during regeneration in the young lead to slightly decreased numbers of MuSCs. This ultimately impairs the regeneration of skeletal muscle and results in a phenotype that partially resembles the one observed in aged regenerating skeletal muscle (Brack and Muñoz-Cánoves, 2016). Interestingly, it was shown that the two ECM molecules Wisp1 and Fibronectin can interact with Itgb1 (Maiese, 2014; Ono et al., 2018). An age-dependent decrease of Fibronectin in the ECM of skeletal muscle has been shown to impair Itgb1 signaling (Rozo et al., 2016). Therefore, we suggest that during aging the balance between different ECM molecules, such as Smoc2, Fibronectin, or Wisp1, is altered, resulting in aberrant activity of membrane receptors in MuSCs, including Itgb1.

CellPress
OPEN ACCESS

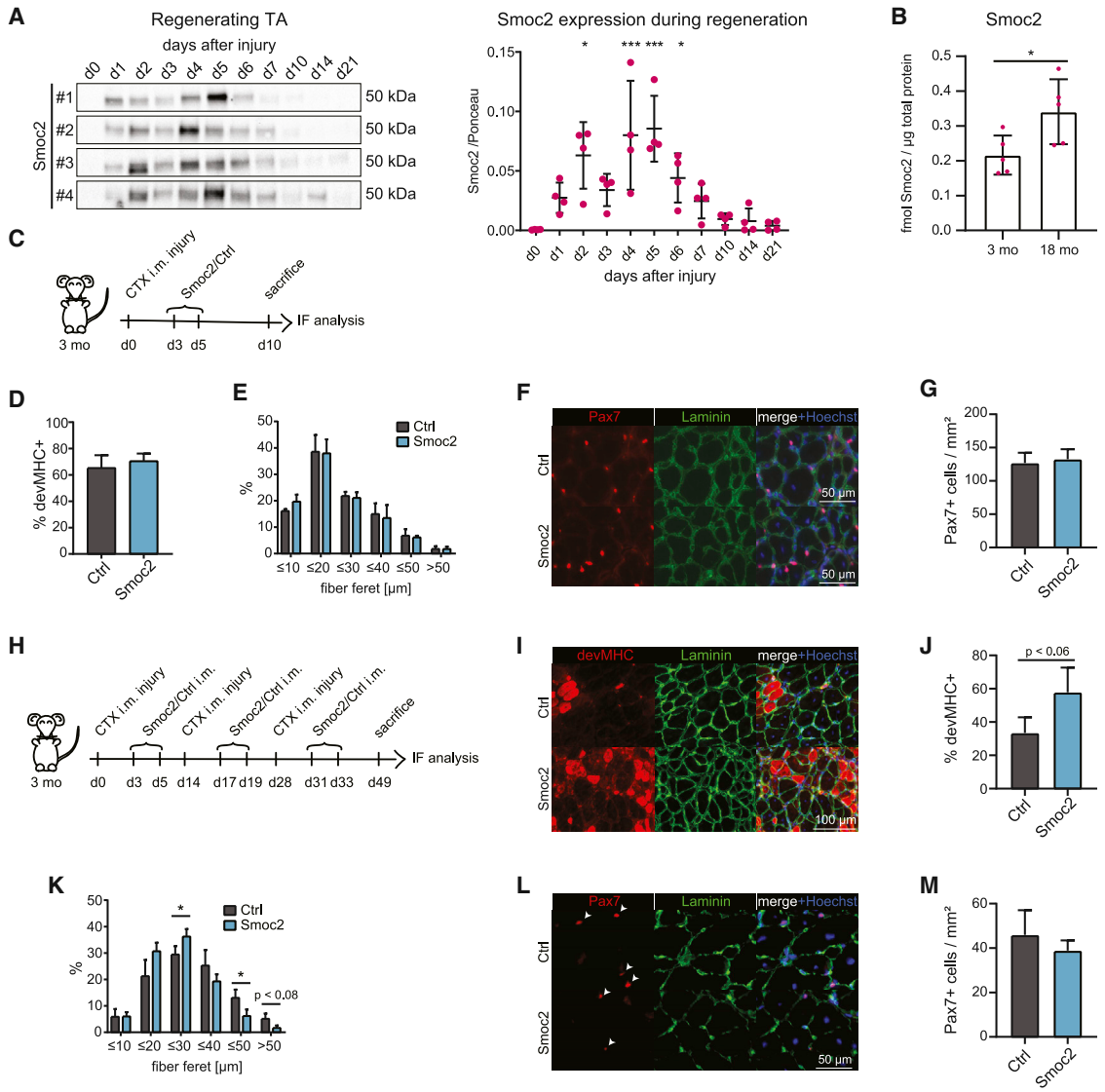

Figure 7. Effect of increased Smoc2 levels on skeletal muscle regeneration

(A) Smoc2 expression in regenerating TA muscles between day 0 (uninjured) and day 21 after injury. n = 4 mice per group, 3 months old. Smoc2 expression was normalized to Ponceau displayed in Figure S7A. ***p < 0.001, *p < 0.05; one-way ANOVA.

(B) Absolute quantification of Smoc2 protein in TA muscle lysates of 3-month-old and 18-month-old mice by parallel reaction monitoring. The concentration of Smoc2 was derived from the average value of 3 peptides quantified (n = 5 per group).

(C) Schematic showing *in vivo* injury; 10 µg Smoc2 or solvent was injected. n = 3 mice per group, 3 months old.

(D) Percentage of regenerating myofibers being positive for devMHC in the injured TA.

(E) Fiber feret distribution of devMHC-positive myofibers.

(F) Representative images for Pax7 (red), Laminin (green), and Hoechst (blue) in regenerating TA muscles. Scale bar: 50 µm.

(G) Quantification of the number of $Pax7^+$ cells normalized to the injured area.

(H) Schematic depicting the repeated injury experiment. The same TA muscle was injured 3 times every 14 days and injected with 10 µg Smoc2 or the solvent after each injury.

(I) Representative images for devMHC (red), Laminin (green), and Hoechst (blue). Scale bar: 100 µm.

(J) Quantification of the percentage of devMHC-positive myofibers of all regenerating fibers. Control: n = 3, Smoc2: n = 4; mice were 2 months old at the start of the experiment.

(K) Fiber feret distribution of devMHC+ myofibers. Control: n = 3, Smoc2: n = 4.

(L) Representative images for Pax7 (red), Laminin (green), and Hoechst (blue) in TA muscle. Scale bar: 50 µm.

(M) Quantification of the number of $Pax7^+$ cells per area in the injured region. n = 3. For (B), (D), (E), (G), (J), (K), and (M), *p < 0.05; two-sided, unpaired Student's t test. Error bars: SD. Related to Figure S10.

In summary, we provide two resources that describe alterations and interactions of protein abundances in MuSCs and their niche during aging. The majority of these changes appear to depend on post-transcriptional mechanisms regulating protein levels. Our data recapitulate known phenotypes of aged MuSCs, including mitochondrial dysfunction, perturbed proteostasis, and altered cell communication, and might therefore help to provide mechanistic insights on how aging impacts the regenerative capacity of MuSCs. We identified Smoc2 as a modulator of the Integrin signaling axis between MuSCs and their niche. Aberrantly high levels of Smoc2, as observed during aging, are sufficient to impair MuSC functionality in young mice following repeated muscle injury. Finally, we propose that targeting the major signaling axis that we identified to be perturbed during aging might represent an efficient strategy to design therapies aimed at improving regeneration of skeletal muscle in the elderly.

STAR★METHODS

Detailed methods are provided in the online version of this paper and include the following:

- KEY RESOURCES TABLE
- RESOURCE AVAILABILITY
  - Lead contact
  - Materials availability
  - Data and code availability
- EXPERIMENTAL MODEL AND SUBJECT DETAILS
  - Mice
  - Cells
- METHOD DETAILS
  - FACS isolation of MuSCs and FAPs
  - Cell culture experiments using FAPs
  - Preparation of MuSCs and FAPs for MS analysis
  - Tissue lysis for immunoblot and MS analysis
  - Data independent acquisition for MuSC and FAP samples
  - Preparation of skeletal muscles for MS analysis
  - TMT labeling
  - High pH peptide fractionation
  - Data acquisition of TMT labeled samples
  - Affinity purification of Smoc2-GFP fusion protein
  - Data acquisition for GFP-trap samples
  - Parallel reaction monitoring for Smoc2
  - Sample preparation for phosphoproteomics analysis
  - Data independent acquisition for enriched phosphopeptides
  - Immunofluorescence analysis of cryo-sections
  - Sirius red staining
  - Floating myofiber culture
  - Immunofluorescence of floating myofibers
  - Proximity labeling assay of MuSCs on floating fiber culture
  - qRT-PCR
  - Immunoblot analysis
  - Cardiotoxin muscle injury and Smoc2 treatment
  - Decellularization of TA tissue
- QUANTIFICATION AND STATISTICAL ANALYSIS
  - Data processing for DIA samples
  - Data processing for TMT labeled samples
  - Data processing for GFP-trap analysis
  - PRM analysis for quantification of Smoc2
  - Data processing for phosphoproteomics
  - Quantification of IF stainings from TA muscles
  - Quantification of IF stainings on floating myofibers
  - Quantification of immunoblots
  - Ingenuity pathway analysis for MuSCs proteome data
  - Analysis and integration of micro array transcriptome data
  - Analysis and integration of RNaseq transcriptome data
  - Analysis of cellular compartments in aging skeletal muscles
  - Analysis and integration of scRNaseq data
  - Network analysis of secreted ligands affected by aging in skeletal muscles and their receptors expressed by MuSCs

SUPPLEMENTAL INFORMATION

Supplemental information can be found online at https://doi.org/10.1016/j.celrep.2021.109223.

ACKNOWLEDGMENTS

The authors gratefully acknowledge support from the FLI Core Facilities Flow Cytometry, Imaging, Proteomics and Mouse as well as the FLI Core Services Histology and Media Preparation. The authors thank Nadia Döhring and Ivonne Heinze for technical assistance, Alexandra Kretz and Diane Penndorf for sharing their mice, Regine Heller for providing the CD31 antibody, Lino Ferreira for technical support, Björn von Eyss and Nadja Gebert for critically proofreading of the manuscript, and Max Tiessen and Domenico Di Fraia for implementing the R shiny webserver. M.H. was supported by a core grant from the Wellcome Trust. This work was supported by a grant from the Deutsche Forschungsgemeinschaft to J.v.M. (MA-3975/2-1). A.O. acknowledges funding from the Deutsche Forschungsgemeinschaft via the Research Training Group ProMoAge (GRK 2155), the Else Kröner-Fresenius-Stiftung (award number 2019_A79), the Deutsches Zentrum für Herz-Kreislaufforschung (award number 81X2800193), and the Fritz Thyssen Foundation (award number 10.20.1.022MN). The FLI is a member of the Leibniz Association and is financially supported by the Federal Government of Germany and the State of Thuringia.

AUTHOR CONTRIBUTIONS

Conceptualization: S.C.S., J.v.M., and A.O.; data curation: S.C.S., J.v.M., and A.O.; experimental procedures: S.C.S., M.S., D.S., and J.v.M.; methodology: S.C.S., J.M.K., D.S., M.H., J.v.M., A.O., and E.C.; project administration: A.O. and J.v.M.; data analysis: S.C.S., P.K., A.O., J.v.M., and S.D.S.; supervision: A.O. and J.v.M.; visualization: S.C.S., D.S., M.H., and A.O.; writing – original draft: S.C.S., J.v.M., and A.O.; writing – review & editing: M.S., J.M.K., D.S., P.K., and M.H.

DECLARATION OF INTERESTS

The authors declare no competing interests.

Received: August 24, 2020
Revised: January 25, 2021
Accepted: May 14, 2021
Published: June 8, 2021

REFERENCES

Alonso-Martin, S., Rochat, A., Mademtzoglou, D., Morais, J., de Reyniès, A., Auradé, F., Chang, T.H.-T., Zammit, P.S., and Relaix, F. (2016). Gene Expression Profiling of Muscle Stem Cells Identifies Novel Regulators of Postnatal Myogenesis. Front. Cell Dev. Biol. *4*, 58.

Baghdadi, M.B., Castel, D., Machado, L., Fukada, S.-I., Birk, D.E., Relaix, F., Tajbakhsh, S., and Mourikis, P. (2018). Reciprocal signalling by Notch-Collagen V-CALCR retains muscle stem cells in their niche. Nature *557*, 714–718.

Benjamini, Y., and Hochberg, Y. (1995). Controlling the False Discovery Rate: A Practical and Powerful Approach to Multiple Testing. J. R. Stat. Soc. B *57*, 289–300.

Bentzinger, C.F., Wang, Y.X., and Rudnicki, M.A. (2012). Building muscle: molecular regulation of myogenesis. Cold Spring Harb. Perspect. Biol. *4*, a008342.

Bentzinger, C.F., Wang, Y.X., Dumont, N.A., and Rudnicki, M.A. (2013a). Cellular dynamics in the muscle satellite cell niche. EMBO Rep. *14*, 1062–1072.

Bentzinger, C.F., Wang, Y.X., von Maltzahn, J., Soleimani, V.D., Yin, H., and Rudnicki, M.A. (2013b). Fibronectin regulates Wnt7a signaling and satellite cell expansion. Cell Stem Cell *12*, 75–87.

Bolstad, B.M., Irizarry, R.A., Astrand, M., and Speed, T.P. (2003). A comparison of normalization methods for high density oligonucleotide array data based on variance and bias. Bioinformatics *19*, 185–193.

Brack, A.S., and Muñoz-Cánoves, P. (2016). The ins and outs of muscle stem cell aging. Skelet. Muscle *6*, 1.

Brack, A.S., Conboy, M.J., Roy, S., Lee, M., Kuo, C.J., Keller, C., and Rando, T.A. (2007). Increased Wnt Signaling During Aging Alters Muscle Stem Cell Fate and Increases Fibrosis. Science *317*, 807–810.

Brosch, M., Yu, L., Hubbard, T., and Choudhary, J. (2009). Accurate and sensitive peptide identification with Mascot Percolator. J. Proteome Res. *8*, 3176–3181.

Bulteau, A.-L., Szweda, L.I., and Friguet, B. (2002). Age-dependent declines in proteasome activity in the heart. Arch. Biochem. Biophys. *397*, 298–304.

Chakkalakal, J.V., and Brack, A.S. (2012). Extrinsic Regulation of Satellite Cell Function and Muscle Regeneration Capacity during Aging. J. Stem Cell Res. Ther. *11*, 001.

Chakkalakal, J.V., Jones, K.M., Basson, M.A., and Brack, A.S. (2012). The aged niche disrupts muscle stem cell quiescence. Nature *490*, 355–360.

Chang, N.C., and Rudnicki, M. a. (2014). Satellite cells: the architects of skeletal muscle. (Elsevier Inc.).

Cirit, M., Grant, K.G., and Haugh, J.M. (2012). Systemic perturbation of the ERK signaling pathway by the proteasome inhibitor, MG132. PLoS One *7*, e50975.

Courcelles, M., Frémin, C., Voisin, L., Lemieux, S., Meloche, S., and Thibault, P. (2013). Phosphoproteome dynamics reveal novel ERK1/2 MAP kinase substrates with broad spectrum of functions. Mol. Syst. Biol. *9*, 669.

Cox, J., and Mann, M. (2008). MaxQuant enables high peptide identification rates, individualized p.p.b.-range mass accuracies and proteome-wide protein quantification. Nat. Biotechnol. *26*, 1367–1372.

Cox, J., Neuhauser, N., Michalski, A., Scheltema, R.A., Olsen, J.V., and Mann, M. (2011). Andromeda: a peptide search engine integrated into the MaxQuant environment. J. Proteome Res. *10*, 1794–1805.

Dobin, A., Davis, C.A., Schlesinger, F., Drenkow, J., Zaleski, C., Jha, S., Batut, P., Chaisson, M., and Gingeras, T.R. (2013). STAR: ultrafast universal RNA-seq aligner. Bioinformatics *29*, 15–21.

Dumont, N.A., Bentzinger, C.F., Sincennes, M.-C., and Rudnicki, M.A. (2015). Satellite Cells and Skeletal Muscle Regeneration. Comprehensive Physiology (John Wiley & Sons, Inc.), pp. 1027–1059.

Edgar, R., Domrachev, M., and Lash, A.E. (2002). Gene Expression Omnibus: NCBI gene expression and hybridization array data repository. Nucleic Acids Res. *30*, 207–210.

Elias, J.E., and Gygi, S.P. (2007). Target-decoy search strategy for increased confidence in large-scale protein identifications by mass spectrometry. Nat. Methods *4*, 207–214.

Ermolaeva, M., Neri, F., Ori, A., and Rudolph, K.L. (2018). Cellular and epigenetic drivers of stem cell ageing. Nat. Rev. Mol. Cell Biol. *19*, 594–610.

Evano, B., and Tajbakhsh, S. (2018). Skeletal muscle stem cells in comfort and stress. NPJ Regen. Med. *3*, 24.

Ferrington, D.A., Husom, A.D., and Thompson, L.V. (2005). Altered proteasome structure, function, and oxidation in aged muscle. FASEB J. *19*, 644–646.

García-Prat, L., Martínez-Vicente, M., Perdiguero, E., Ortet, L., Rodríguez-Ubreva, J., Rebollo, E., Ruiz-Bonilla, V., Gutarra, S., Ballestar, E., Serrano, A.L., et al. (2016). Autophagy maintains stemness by preventing senescence. Nature *529*, 37–42.

García-Prat, L., Perdiguero, E., Alonso-Martín, S., Dell'Orso, S., Ravichandran, S., Brooks, S.R., Juan, A.H., Campanario, S., Jiang, K., Hong, X., et al. (2020). FoxO maintains a genuine muscle stem-cell quiescent state until geriatric age. Nat. Cell Biol. *22*, 1307–1318.

Giordani, L., He, G.J., Negroni, E., Sakai, H., Law, J.Y.C., Siu, M.M., Wan, R., Corneau, A., Tajbakhsh, S., Cheung, T.H., and Le Grand, F. (2019). High-Dimensional Single-Cell Cartography Reveals Novel Skeletal Muscle-Resident Cell Populations. Mol. Cell *74*, 609–621.e6.

Heinze, I., Bens, M., Calzia, E., Holtze, S., Dakhovnik, O., Sahm, A., Kirkpatrick, J.M., Szafranski, K., Romanov, N., Sama, S.N., et al. (2018). Species comparison of liver proteomes reveals links to naked mole-rat longevity and human aging. BMC Biol. *16*, 82.

Hüttner, S.S., Ahrens, H.E., Schmidt, M., Henze, H., Jung, M.J., Schüler, S.C., and von Maltzahn, J. (2019). Isolation and Culture of Individual Myofibers and Their Adjacent Muscle Stem Cells from Aged and Adult Skeletal Muscle. Methods Mol. Biol. *2045*, 25–36.

Janssens, G.E., Meinema, A.C., González, J., Wolters, J.C., Schmidt, A., Guryev, V., Bischoff, R., Wit, E.C., Veenhoff, L.M., and Heinemann, M. (2015). Protein biogenesis machinery is a driver of replicative aging in yeast. eLife *4*, e08527.

Kelmer Sacramento, E., Kirkpatrick, J.M., Mazzetto, M., Baumgart, M., Bartolome, A., Di Sanzo, S., Caterino, C., Sanguanini, M., Papaevgeniou, N., Lefaki, M., et al. (2020). Reduced proteasome activity in the aging brain results in ribosome stoichiometry loss and aggregation. Mol. Syst. Biol. *16*, e9596.

Kitajima, Y., Suzuki, N., Nunomiya, A., Osana, S., Yoshioka, K., Tashiro, Y., Takahashi, R., Ono, Y., Aoki, M., and Nagatomi, R. (2018). The Ubiquitin-Proteasome System Is Indispensable for the Maintenance of Muscle Stem Cells. Stem Cell Reports *11*, 1523–1538.

Kiyatkin, A., Aksamitiene, E., Markevich, N.I., Borisov, N.M., Hoek, J.B., and Kholodenko, B.N. (2006). Scaffolding protein Grb2-associated binder 1 sustains epidermal growth factor-induced mitogenic and survival signaling by multiple positive feedback loops. J. Biol. Chem. *281*, 19925–19938.

Lacraz, G., Rouleau, A.J., Couture, V., Söllrald, T., Drouin, G., Veillette, N., Grandbois, M., and Grenier, G. (2015). Increased stiffness in aged skeletal muscle impairs muscle progenitor cell proliferative activity. PLoS One *10*, e0136217.

Larsson, L., Biral, D., Campione, M., and Schiaffino, S. (1993). An age-related type IIB to IIX myosin heavy chain switching in rat skeletal muscle. Acta Physiol. Scand. *147*, 227–234.

Lee, J.T.H., Patikas, N., Kiselev, V.Y., and Hemberg, M. (2019). Fast searches of large collections of single cell data using scfind. bioRxiv. https://doi.org/10.1101/788596.

Lepper, C., Partridge, T.A., and Fan, C.M. (2011). An absolute requirement for Pax7-positive satellite cells in acute injury-induced skeletal muscle regeneration. Development *138*, 3639–3646.

Li, L., Rozo, M., Yue, S., Zheng, X., J Tan, F., Lepper, C., and Fan, C.M. (2019). Muscle stem cell renewal suppressed by Gas1 can be reversed by GDNF in mice. Nat. Metab. *1*, 985–995.

Liao, Y., Smyth, G.K., and Shi, W. (2014). featureCounts: an efficient general purpose program for assigning sequence reads to genomic features. Bioinformatics *30*, 923–930.

Liao, Y., Wang, J., Jaehnig, E.J., Shi, Z., and Zhang, B. (2019). WebGestalt 2019: gene set analysis toolkit with revamped UIs and APIs. Nucleic Acids Res. *47*, W199–W205.

Liu, P., Lu, J., Cardoso, W.V., and Vaziri, C. (2008). The SPARC-related factor SMOC-2 promotes growth factor-induced cyclin D1 expression and DNA synthesis via integrin-linked kinase. Mol. Biol. Cell *19*, 248–261.

Liu, L., Cheung, T.H., Charville, G.W., Hurgo, B.M.C., Leavitt, T., Shih, J., Brunet, A., and Rando, T.A. (2013). Chromatin modifications as determinants of muscle stem cell quiescence and chronological aging. Cell Rep. *4*, 189–204.

Love, M.I., Huber, W., and Anders, S. (2014). Moderated estimation of fold change and dispersion for RNA-seq data with DESeq2. Genome Biol. *15*, 550.

Lukjanenko, L., Jung, M.J., Hegde, N., Perruisseau-Carrier, C., Migliavacca, E., Rozo, M., Karaz, S., Jacot, G., Schmidt, M., Li, L., et al. (2016). Loss of fibronectin from the aged stem cell niche affects the regenerative capacity of skeletal muscle in mice. Nat. Med. *22*, 897–905.

Lukjanenko, L., Karaz, S., Stuelsatz, P., Gurriaran-Rodriguez, U., Michaud, J., Dammone, G., Sizzano, F., Mashinchian, O., Ancel, S., Migliavacca, E., et al. (2019). Aging Disrupts Muscle Stem Cell Function by Impairing Matricellular WISP1 Secretion from Fibro-Adipogenic Progenitors. Cell Stem Cell *24*, 433–446.e7.

Maiese, K. (2014). WISP1: Clinical insights for a proliferative and restorative member of the CCN family. Curr. Neurovasc. Res. *11*, 378–389.

Mashinchian, O., Pisconti, A., Le Moal, E., and Bentzinger, C.F. (2018). The Muscle Stem Cell Niche in Health and Disease. Current Topics in Developmental Biology (Elsevier Inc.), pp. 23–65.

Morris, J.H., Kuchinsky, A., Ferrin, T.E., and Pico, A.R. (2014). enhancedGraphics: a Cytoscape app for enhanced node graphics. F1000Res. *3*, 147.

Murphy, M.M., Lawson, J.A., Mathew, S.J., Hutcheson, D.A., and Kardon, G. (2011). Satellite cells, connective tissue fibroblasts and their interactions are crucial for muscle regeneration. Development *138*, 3625–3637.

Ono, M., Masaki, A., Maeda, A., Kilts, T.M., Hara, E.S., Komori, T., Pham, H., Kuboki, T., and Young, M.F. (2018). CCN4/WISP1 controls cutaneous wound healing by modulating proliferation, migration and ECM expression in dermal fibroblasts via α5β1 and TNFα. Matrix Biol. *68–69*, 533–546.

Ori, A., Toyama, B.H., Harris, M.S., Bock, T., Iskar, M., Bork, P., Ingolia, N.T., Hetzer, M.W., and Beck, M. (2015). Integrated Transcriptome and Proteome Analyses Reveal Organ-Specific Proteome Deterioration in Old Rats. Cell Syst. *1*, 224–237.

Parca, L., Beck, M., Bork, P., and Ori, A. (2018). Quantifying compartment-associated variations of protein abundance in proteomics data. Mol. Syst. Biol. *14*, e8131.

Pasut, A., Oleynik, P., and Rudnicki, M.A. (2012). Isolation of muscle stem cells by fluorescence activated cell sorting cytometry. Methods Mol. Biol. *798*, 53–64.

Perez-Riverol, Y., Csordas, A., Bai, J., Bernal-Llinares, M., Hewapathirana, S., Kundu, D.J., Inuganti, A., Griss, J., Mayer, G., Eisenacher, M., et al. (2019). The PRIDE database and related tools and resources in 2019: improving support for quantification data. Nucleic Acids Res. *47*, D442–D450.

Pisco, A.O., Schaum, N., McGeever, A., Karkanias, J., Neff, N.F., Darmanis, S., Wyss-Coray, T., and Quake, S.R. (2019). A Single Cell Transcriptomic Atlas Characterizes Aging Tissues in the Mouse. bioRxiv. https://doi.org/10.1101/661728.

Post, H., Penning, R., Fitzpatrick, M.A., Garrigues, L.B., Wu, W., MacGillavry, H.D., Hoogenraad, C.C., Heck, A.J.R., and Altelaar, A.F.M. (2017). Robust, Sensitive, and Automated Phosphopeptide Enrichment Optimized for Low Sample Amounts Applied to Primary Hippocampal Neurons. J. Proteome Res. *16*, 728–737.

Price, F.D., von Maltzahn, J., Bentzinger, C.F., Dumont, N.A., Yin, H., Chang, N.C., Wilson, D.H., Frenette, J., and Rudnicki, M.A. (2014). Inhibition of JAK-STAT signaling stimulates adult satellite cell function. Nat. Med. *20*, 1174–1181.

Pronsato, L., Boland, R., and Milanesi, L. (2012). Testosterone exerts antiapoptotic effects against H2O2 in C2C12 skeletal muscle cells through the apoptotic intrinsic pathway. J. Endocrinol. *212*, 371–381.

R Development Core Team (2018). R: A language and environment for statistical computing (R Foundation for Statistical Computing).

Ramilowski, J.A., Goldberg, T., Harshbarger, J., Kloppmann, E., Lizio, M., Satagopam, V.P., Itoh, M., Kawaji, H., Carninci, P., Rost, B., and Forrest, A.R. (2015). A draft network of ligand-receptor-mediated multicellular signalling in human. Nat. Commun. *6*, 7866.

Rayagiri, S.S., Ranaldi, D., Raven, A., Mohamad Azhar, N.I.F., Lefebvre, O., Zammit, P.S., and Borycki, A.-G. (2018). Basal lamina remodeling at the skeletal muscle stem cell niche mediates stem cell self-renewal. Nat. Commun. *9*, 1075.

Ritchie, M.E., Phipson, B., Wu, D., Hu, Y., Law, C.W., Shi, W., and Smyth, G.K. (2015). limma powers differential expression analyses for RNA-sequencing and microarray studies. Nucleic Acids Res. *43*, e47.

Rocnik, E.F., Liu, P., Sato, K., Walsh, K., and Vaziri, C. (2006). The novel SPARC family member SMOC-2 potentiates angiogenic growth factor activity. J. Biol. Chem. *281*, 22855–22864.

Rogers, R., Baumann, C., and Otis, J. (2015). Recovery of skeletal muscle function following injury is not augmented by acute resveratrol supplementation. Int. J. Clin. Exp. Physiol. *2*, 29.

Rozo, M., Li, L., and Fan, C.-M. (2016). Targeting β1-integrin signaling enhances regeneration in aged and dystrophic muscle in mice. Nat. Med. *22*, 889–896.

Ryall, J.G., Dell'Orso, S., Derfoul, A., Juan, A., Zare, H., Feng, X., Clermont, D., Koulnis, M., Gutierrez-Cruz, G., Fulco, M., and Sartorelli, V. (2015). The NAD(+)-dependent SIRT1 deacetylase translates a metabolic switch into regulatory epigenetics in skeletal muscle stem cells. Cell Stem Cell *16*, 171–183.

Saclier, M., Yacoub-Youssef, H., Mackey, A.L., Arnold, L., Ardjoune, H., Magnan, M., Sailhan, F., Chelly, J., Pavlath, G.K., Mounier, R., et al. (2013). Differentially activated macrophages orchestrate myogenic precursor cell fate during human skeletal muscle regeneration. Stem Cells *31*, 384–396.

Sambasivan, R., Yao, R., Kissenpfennig, A., Van Wittenberghe, L., Paldi, A., Gayraud-Morel, B., Guenou, H., Malissen, B., Tajbakhsh, S., and Galy, A. (2011). Pax7-expressing satellite cells are indispensable for adult skeletal muscle regeneration. Development *138*, 3647–3656.

Schiaffino, S., and Reggiani, C. (2011). Fiber types in mammalian skeletal muscles. Physiol. Rev. *91*, 1447–1531.

Schmidt, M., Schüler, S.C., Hüttner, S.S., von Eyss, B., and von Maltzahn, J. (2019). Adult stem cells at work: regenerating skeletal muscle. Cell. Mol. Life Sci. *76*, 2559–2570.

Schneider, C.A., Rasband, W.S., and Eliceiri, K.W. (2012). NIH Image to ImageJ: 25 Years of Image Analysis. Nature Methods *9*, 671–675.

Schüler, S.C., Gebert, N., and Ori, A. (2020). Stem cell aging: The upcoming era of proteins and metabolites. Mech. Ageing Dev. *190*, 111288.

Serrano, A.L., Mann, C.J., Vidal, B., Ardite, E., Perdiguero, E., and Muñoz-Cánoves, P. (2011). Cellular and Molecular Mechanisms Regulating Fibrosis in Skeletal Muscle Repair and Disease. Curr. Top. Dev. Biol. *96*, 167–201.

Shannon, P., Markiel, A., Ozier, O., Baliga, N.S., Wang, J.T., Ramage, D., Amin, N., Schwikowski, B., and Ideker, T. (2003). Cytoscape: a software environment for integrated models of biomolecular interaction networks. Genome Res. *13*, 2498–2504.

Silva, A.C., Rodrigues, S.C., Caldeira, J., Nunes, A.M., Sampaio-Pinto, V., Resende, T.P., Oliveira, M.J., Barbosa, M.A., Thorsteinsdóttir, S., Nascimento, D.S., and Pinto-do-Ó, P. (2016). Three-dimensional scaffolds of fetal decellularized hearts exhibit enhanced potential to support cardiac cells in comparison to the adult. Biomaterials *104*, 52–64.

Sousa-Victor, P., Gutarra, S., García-Prat, L., Rodriguez-Ubreva, J., Ortet, L., Ruiz-Bonilla, V., Jardí, M., Ballestar, E., González, S., Serrano, A.L., et al. (2014). Geriatric muscle stem cells switch reversible quiescence into senescence. Nature *506*, 316–321.

Sousa-Victor, P., García-Prat, L., Serrano, A.L., Perdiguero, E., and Muñoz-Cánoves, P. (2015). Muscle stem cell aging: regulation and rejuvenation. Trends Endocrinol. Metab. *26*, 287–296.

Strimmer, K. (2008). A unified approach to false discovery rate estimation. BMC Bioinformatics *9*, 303.

Su, J.-R., Kuai, J.-H., and Li, Y.-Q. (2016). Smoc2 potentiates proliferation of hepatocellular carcinoma cells *via* promotion of cell cycle progression. World J. Gastroenterol. *22*, 10053–10063.

Svendsen, A.F., Yang, D., Lazare, S., Zwart, E., Ausema, A., de Haan, G., and Bystrykh, L.V. (2020). A comprehensive transcriptome signature of murine hematopoietic stem cell aging. bioRxiv. https://doi.org/10.1101/2020.08.10.244434.

Szklarczyk, D., Gable, A.L., Lyon, D., Junge, A., Wyder, S., Huerta-Cepas, J., Simonovic, M., Doncheva, N.T., Morris, J.H., Bork, P., et al. (2019). STRING v11: protein-protein association networks with increased coverage, supporting functional discovery in genome-wide experimental datasets. Nucleic Acids Res. *47*, D607–D613.

Theret, M., Mounier, R., and Rossi, F. (2019). The origins and non-canonical functions of macrophages in development and regeneration. Development *146*, dev156000.

Tierney, M.T., Aydogdu, T., Sala, D., Malecova, B., Gatto, S., Puri, P.L., Latella, L., and Sacco, A. (2014). STAT3 signaling controls satellite cell expansion and skeletal muscle repair. Nat. Med. *20*, 1182–1186.

Wei, Y.-N., Hu, H.-Y., Xie, G.-C., Fu, N., Ning, Z.-B., Zeng, R., and Khaitovich, P. (2015). Transcript and protein expression decoupling reveals RNA binding proteins and miRNAs as potential modulators of human aging. Genome Biol. *16*, 41.

Wosczyna, M.N., and Rando, T.A. (2018). A Muscle Stem Cell Support Group: Coordinated Cellular Responses in Muscle Regeneration. Dev. Cell *46*, 135–143.

Zhang, H., Ryu, D., Wu, Y., Gariani, K., Wang, X., Luan, P., D'Amico, D., Ropelle, E.R., Lutolf, M.P., Aebersold, R., et al. (2016). NAD+ repletion improves mitochondrial and stem cell function and enhances life span in mice. Science *352*, 1436–1443.

Zismanov, V., Chichkov, V., Colangelo, V., Jamet, S., Wang, S., Syme, A., Koromilas, A.E., and Crist, C. (2016). Phosphorylation of eIF2α Is a Translational Control Mechanism Regulating Muscle Stem Cell Quiescence and Self-Renewal. Cell Stem Cell *18*, 79–90.

STAR★METHODS

KEY RESOURCES TABLE

REAGENT or RESOURCE	SOURCE	IDENTIFIER
Antibodies		
anti-alpha 7 integrin 647 (clone: R2F2)	The University Of British Columbia AbLab	67-0010-05
Polyclonal goat IgG Bcam	R&D	AF8299 RRID:AB_2811217
Polyclonal rabbit IgG Calcr	Biorad	AHP635 RRID:AB_2068967
Rat IgG2b CD11b-PE	BD Bioscience	553311 RRID:AB_394775
Rat IgG2a CD31-PE	BD Bioscience	553373 RRID:AB_394819
Rat IgG2b CD45-PE	BD Bioscience	553081 RRID:AB_394611
Polyclonal rabbit IgG Col14a1	Abcam	Ab101464 RRID:AB_10710544
Hybridoma mouse IgG1 devMHC	DSHB	clone F.1652 RRID:AB_528358
Polyclonal rabbit IgG Elastin	Abcam	ab217356 RRID:AB_2827685
Monoclonal mouse IgG2b Erk1	Santa Cruz	sc-271269 RRID:AB_10611091
Monoclonal mouse IgG2b Erk2	Santa Cruz	sc-1647 RRID:AB_627547
Monoclonal mouse IgG1 Gapdh	Santa Cruz	sc-365062 RRID:AB_10847862
Polyclonal rabbit IgG laminin	Sigma	L9393 RRID:AB_477163
Monoclonal rat IgG2a MyoD	Merck	MABE132 RRID:AB_2665561
Hybridoma mouse IgG1 Pax7	DSHB	Pax7 RRID:AB_528428
Polyclonal goat IgG Pdgfrα	R&D	AF1062 RRID:AB_2236897
Polyclonal rabbit IgG pErk1/2	Cell Signaling	4370 RRID:AB_2315112
Monoclonal rat IgG2a Sca1-FITC	eBioscience	11-5981-85 RRID:AB_465334
Monoclonal rat IgG2a Sca1-PE (Ly-6A/E-PE)	BD Bioscience	553108 RRID:AB_394629
Monoclonal mouse IgG2a Smoc2	Santa Cruz	sc-376104 RRID:AB_10989756
Polyclonal rabbit IgG Smoc2	MyBiosource	MBS2527784
Polyclonal rabbit IgG Sun2	Atlas antibodies	HPA001209 RRID:AB_1080465
Chemicals, peptides, and recombinant proteins		
Cardiotoxin	Latoxan	L8102
HRM peptides	Biognosys AG	42896
Recombinant mouse SMOC-2 protein	R&D	6075-SM-050
Peptide: smoc2 FSALTFLR	JPT	customized
Peptide: smoc2 LSEPDPSHTLEER	JPT	customized
Peptide: smoc2 DPQLEIAHR	JPT	customized
Duolink blocking solution	Sigma	DUO82007-8ml
Duolink in situe detection reagents RED	Sigma	DUO92008-100RXN
Probemaker MINUS	Sigma	DUO9201-1KT
Probemaker PLUS	Sigma	DUO92009-1KT
Critical commercial assays		
GFP-Trap	Chromotek	gta-100
TMT10plex reagents	Thermo Fisher	90111
AssayMAP Fe(III)-NTA cartridges	Agilent Technologies	G5496-60085
Deposited data		
Proteomics datasets for skeletal muscle aging	ProteomeXchange	PXD015616
Proteomics datasets for GFP trap analysis	ProteomeXchange	PXD015728

(*Continued on next page*)

Continued

REAGENT or RESOURCE	SOURCE	IDENTIFIER
Proteomics datasets for MuSC aging	ProteomeXchange	PXD016356
Proteomics datasets for Monensin treatment of FAPs	ProteomeXchange	PXD023628
Phosphoproteomics dataset	ProteomeXchange	PXD023643
Experimental models: cell lines		
C2C12	ATCC	ATCC® CRL-1772
HEK293 (Flp-In 293 T-Rex cells)	Thermo Fisher	R78007
HEK293-GFP	This paper	N/A
HEK293-Smoc2-GFP	This paper	N/A
Oligonucleotides		
For primer sequences see Table S8	Metabion	Customized
siRNA targeting Itgb1 (ON-Target plus SMART pool)	Dharmacon	L-040783-01-0005
Non targetin siRNA (ON-Target plus SMART pool)	Dharmacon	D-001810-10-05
Recombinant DNA		
Mouse Smoc2	Dharmacon	MMM1013-202764967
Software and algorithms		
Compartment normalized value analysis	Parca et al., 2018	N/A
Cytoscape v.3.8.0	Shannon et al., 2003	N/A
DESeq2 package for R	Love et al., 2014	N/A
FeatureCounts v1.6.5	Liao et al., 2014	N/A
ImageJ	(Schneider et al., 2012)	N/A
Ingenuity pathway analysis software v.01-14	QIAGEN	830018
limma package	Ritchie et al., 2015	N/A
Mascot v2.5.1	Matrix Science	N/A
MaxQuant v1.5.3.28 with Andromeda search engine	Max Planck Institute of Biochemistry	Cox et al., 2011
GraphPad Prism v8.3.0	GraphPad	RRID: SCR_002798
Proteome Discoverer v2.0	Thermo Fisher	OPTON-30812
R v3.3.3, v3.4.1, v3.6.3, v4.0.1	R Development Core Team, 2018	RRID: SCR_000432
RStudio v. 1.2.5042	RstudioTeam	http://www.rstudio.com/
scfind	Lee et al., 2019	N/A
SpectroDive v9	Biognosys AG	N/A
Spectronaut v10-14	Biognosys AG	Sw-3001
STAR v2.7.6a	Dobin et al., 2013	N/A
Zen v3.0	Zeiss	N/A
Other		
R shiny web app for proteomics data	This paper	https://genome.leibniz-fli.de/shiny/orilab/muscle-aging/

RESOURCE AVAILABILITY

Lead contact

Further information and requests for resources and reagents should be directed to and will be fulfilled by the Lead Contact Julia von Maltzahn (Julia.vonMaltzahn@leibniz-fli.de).

Materials availability

Plasmids and cell lines generated in this study can be obtained by contacting the Lead Contact. Further information and requests for resources and reagents should be directed to and will be fulfilled by the Lead Contact Julia von Maltzahn (Julia.vonMaltzahn@leibniz-fli.de).

Data and code availability

The mass spectrometry proteomics data have been deposited to the ProteomeXchange Consortium via the PRIDE (Perez-Riverol et al., 2019) partner repository with the dataset identifier PRIDE: PXD015616, PXD015728, PXD016356, PXD023628, PXD023643

In addition, the proteomics data presented in this manuscript are available via a R shiny web server: https://genome.leibniz-fli.de/shiny/orilab/muscle-aging/

The codes supporting the study are available from the corresponding authors upon request.

EXPERIMENTAL MODEL AND SUBJECT DETAILS

All animal experiments were carried out with the approval of the Thüringer Landesamt für Verbraucherschutz (Germany) (Reg.-Nr. 011-03/14, FLI-17-014 and FLI-18-006).

Mice

All wild-type mice were C57BL/6J obtained from Janvier or from internal breeding at the Leibniz Institute on Aging – Fritz Lipmann Institute (FLI) using the Janvier strain. All animals were kept in groups in a specific pathogen-free animal facility with a constant 12 h light/dark cycle and fed *ad libitum*. Young mice were aged 2-3 months, old mice were aged 18-20 months and geriatric animals were aged 24-42 months. All mice used in this study were male.

Cells

Muscle stem cells (MuSCs) were isolated from young, old and geriatric mice as described in the section "FACS Isolation of MuSCs and FAPs" below.

Myoblasts were isolated from male C57BL/6J mice with an age of 5 months and cultured on collagen (Corning #354236) coated plates in Ham's F-10 Nutrient Mix (Thermo Fisher #31550031) supplemented with 10% FBS (Thermo Fisher #10270106), 1% Penicillin-Streptomycin (Thermo Fisher #15140-122) and 2.5 ng/ml bFGF (Thermo Fisher #13256029) in a 37°C incubator with 95% humidity and 5% CO2.

Fibro-adipogenic-progenitor cells (FAPs) for qRT-PCR analysis were isolated from 2 and 25 months old, male C57BL/6J mice and immediately frozen as described in the section "FACS Isolation of MuSCs and FAPs."

FAPs for cell culture experiments were isolated from 2 – 3 months old, male C57BL/6J mice and cultured in DMEM high glucose (Sigma #D6429) supplemented with 10% FBS (Thermo Fisher #10270106), 1% Penicillin-Streptomycin (Thermo Fisher #15140-122) and 2.5 ng/ml bFGF (Thermo Fisher #13256029) in a 37°C incubator with 95% humidity and 5% CO2.

C2C12 cells were obtained from ATCC (ATCC® CRL-1772) and cultured in DMEM high glucose (Sigma #D6429) supplemented with 10% FBS (Thermo Fisher #10270106), 1% Penicillin-Streptomycin (Thermo Fisher #15140-122) in a 37°C incubator with 95% humidity and 5% CO2.

HEK293 cells (Flp-In 293 T-Rex cells) were obtained from Thermo Fisher (R78007). HEK293 cells were grown in Dulbecco's modified Eagle's medium (Sigma #D6429) with high glucose (5 g/l) supplemented with 10% heat inactivated fetal bovine serum (Thermo Fisher #10270106) and supplementation with 100 μg/ml Zeocin (Thermo Fisher #R250-01) and 15 μg/ml Blasticidin (Thermo Fisher #R210-01). After generation of a stable line cells were supplemented with 100 μg/ml Hygromycin (Thermo Fisher # 10687-010) and 15 μg/ml Blasticidin. Cells were cultured in a 37°C incubator with 95% humidity and 5% CO2.

METHOD DETAILS

FACS isolation of MuSCs and FAPs

MuSCs and FAPs were isolated from hindlimb muscles of adult male mice of different ages. The muscles were dissected and collected in PBS, minced using scissors and digested in 2.5 g/ml collagenase B (Sigma) and 1 g/ml dispase (Sigma) for 20 min at 37°C. Together with 12 mL of isolation medium (HAMs F10 + 20%FBS) the digested muscle pieces were transferred into a 15 mL tube (188271, Corning) to allow the sedimentation of larger undigested muscle chunks. The sample was then filtered using a 0.74 μm cell strainer (Corning) into a 50 mL tube, spun down at 450x *g* (Centrifuge 5408R, Eppendorf) for 5 min at room temperature and resuspended in 500 μL isolation medium. The sample was then incubated on ice for 15 min with the antibodies used for FACS analysis, as indicated below. Afterward, 15 mL PBS were added, the sample was spun down for 5 min at 450x *g* at room temperature followed by resuspension in 1 mL PBS. After filtering the cells with a 0.35 μm cell strainer (Corning), a staining with SYTOX Blue Dead Cell Stain (Thermo Fisher) was performed to distinguish between dead and alive cells. A BD FACSAria III was used for sorting of the cells.

For MuSCs, gating was set to select for Sca1- (Ly-6A/E-PE, 553108, BD Bioscience, 1:500), CD11b- (CD11b-PE, BD Bioscience, order: 553311, 1:500), CD31- (CD31-PE, BD Bioscience, order: 553373, 1:500), CD45- (CD45-PE, BD Bioscience, order:553081, 1:500) and alpha7-integrin+ (anti-Alpha 7 Integrin 647 (clone: R2F2), The University Of British Columbia AbLab, order: 67-0010-05, 1:500) cells. For further proteomics analysis isolated MuSCs were collected directly into 2x lysis buffer (100 mM HEPES pH8, 20 mM dithiotreitol, 2% sodium dodecyl sulfate) and stored at −80°C.

For FAPs, gating was set to select for Sca1+ (Sca1-FITC, eBioscience #11-5981-85, 1:500), CD11b- (CD11b-PE, BD Bioscience #553311, 1:500), CD31- (CD31-PE, BD Bioscience #553373, 1:500), CD45- (CD45-PE, BD Bioscience #553081, 1:500) and alpha7-integrin- (anti-Alpha 7 Integrin 647 (clone: R2F2), The University Of British Columbia AbLab #67-0010-05, 1:500) cells. FAPs were collected in 10% FBS in PBS, spun down 450x *g* for 5 min and cells were either taken into culture as described above or frozen at −20°C.

Cell culture experiments using FAPs

All experiments with FAPs were performed with cells which were passaged three times at the maximum. For targeted proteomic analysis of conditioned media from FAPs the supernatant was collected 48 h after seeding the cells. Monensin (GolgiStop, BD # 554724) treatment was performed as described according to the instructions provided by the manufacturer (0.33 µl Monensin in 500 µl medium, final 0.00017% Monensin) for 4 h and 8 h. Cells were collected and lysed in RIPA buffer (150 mM Sodium Chloride (Roth #P029.2), 1% Triton X-100 (v/v, Roth #3051.3), 0.5% Sodium Deoxycholate (Thermo Fisher #89904), 0.1% SDS (w/v, Sigma #75746-250G), 50 mM Tris (Roth #4855.2), pH8) for further analysis.

Preparation of MuSCs and FAPs for MS analysis

Samples from FACS were sonicated 10x 1 min using a Bioruptor Plus (Diagenode) on high intensity at 20°C to lyse the cells, boiled for 10 min at 95°C using a block heater and sonicated again 10x 1 min as before. Proteins were reduced with 10 mM dithioreitol (Roth #6908.3) for 30 min at 37°C followed by alkylation with 15 mM iodoacetamide (Sigma #I1149) for 30 min at room temperature in the dark. Subsequently, proteins were precipitated with 100% Acetone (Biosolve # 0001037801BS) over night at −20°C. Then, samples were spun down at 21,000x *g*, 30 min, 4°C, the pellet was washed with 80% acetone (v/v), spun down at 21,000x *g*, 10 min, 4°C, washed again with 80% acetone (v/v) and spun down at 21,000x *g* for 2 min at 4°C. The pellets were air-dried and resuspended in 30 µL M Urea (Sigma #U6504), 100 mM HEPES (Sigma #H3375), pH8 by sonication for 3x 1 min using a Bioruptor Plus. Lysyl endopeptidase (Lys-C, Wako Chemical GmbH #125- 05061) was added at a 1:100 enzyme:protein ratio followed by incubation for 4 h at 37°C with continuous shaking at 650 rpm. Samples were then diluted 1:1 with HPLC grade water (Sigma #270733) and trypsin (Promega #V5111) added at a 1:100 enzyme:protein ratio. The samples were digested for 16 h at 37°C at 650 rpm under continuous shaking. The digested samples were acidified by the addition of trifluoroacetic acid (Biosolve #0020234131BS) to a final concentration of 2% (v/v) and then desalted using Waters Oasis® HLB µElution Plate 30 µm (Waters #186001828BA) according to the manufacturer's instructions. The eluates were dried with a speed vacuum centrifuge and peptides were reconstituted in 8.5 µl reconstitution buffer (5% (v/v) acetonitrile (Biosolve #0001204102BS), 0.1% (v/v) formic acid (Roth #4724.3) in Milli-Q water), 0.5 µL of the HRM kit (Biognosys #Ki-3002-1) was added in the dilution recommended by the manufacturer and 1 µg of peptides were injected for measurement in the mass spectrometer.

Tissue lysis for immunoblot and MS analysis

Skeletal muscle samples were cut into pieces inside a Precellys Keramik-Kit 1,4/2,8 mm tube (VWR # 431-0170), the respective volume of PBS was added (Gastrocnemius: 800 µl, TA: 400 µl, Soleus: 300 µl, EDL: 400 µl) and samples were homogenized using in a Precellys 24 homogenizer (Bertin) for 30 s at 4°C. For a second round of homogenization (also 30 s), an additional volume of 400 µL PBS was added to Gastrocnemius samples, while 200 µL of PBS were added to TA samples. All muscle samples were aliquoted before subsequent lysis (Gastrocnemius: 20 µl, TA: 25 µl, Soleus: 30 µL and EDL: 30 µl). For lysis, the sample volume was adjusted to to 100 µL with PBS followed by addition of 20 µL of 10% (w/v) sodium deoxycholate (Sigma #30970) before boiling at 95°C for 10 min. Samples were then allowed to cool down at room temperature for 10 min, then 80 µL of 10M Urea (Sigma #46504) in 250 mM ammonium bicarbonate (Roth #T871.2) were added. Samples were sonicated with a Bioruptor Plus for 10x 1 min on, 30 s off at 20°C using the highest settings. Samples were spun down at 21,000x *g* for 1 min and transferred into a new 1.5 mL tube. SDS-PAGE and BCA assay were performed to estimate the protein concentration of each sample.

Data independent acquisition for MuSC and FAP samples

For spectral library generation, a pool of approx. 1 µg of reconstituted peptides was analyzed using Data Dependent Acquisition (DDA) using the nanoAcquity UPLC system (Waters) equipped with a trapping (nanoAcquity Symmetry C18, 5 µm, 180 µm x 20mm, Waters) and an analytical column (nanoAcquity BEH C18, 2.5 µm, 75 µm x 250 mm, 186007484, Waters). The outlet of the analytical column was coupled directly to an Orbitrap Fusion Lumos (Thermo Fisher) using the Proxeon nanospray source. The samples were loaded with a constant flow of solvent A (0.1% formic acid (v/v, 4724.3, Roth). Peptides were eluted via a non-linear gradient from 0% to 40% solution B (0.1% formic acid (v/v, 4724.3, Roth) in acetonitrile (0001204102BS, Biosolve)) in 120min. The peptides were introduced into the mass spectrometer via a Pico-Tip Emitter 360 µm OD x 20 µm ID; 10 µm tip (FS360-20-10-D-20, New Objective). Total run time was 145min, including clean-up and column re-equilibration. The RF lens was set to 30%. For spectral library generation, individual MuSC samples were measured in DDA mode. The conditions for DDA data acquisition were as follows: Full scan MS spectra with mass range 350-1650 m/z were acquired in profile mode in the Orbitrap with a

resolution of 60,000 FWHM. The filling time was set at maximum of 50 ms with limitation of 2×10^5 ions. The "Top Speed" method was employed to take the maximum number of precursor ions (with an intensity threshold of 5×10^4) from the full scan MS for fragmentation (using HCD collision energy, 30%) and quadrupole isolation (1.4 Da window) and measurement in the Orbitrap (resolution 15,000 FWHM, fixed first mass 120 m/z), with a cycle time of 3 s. The MIPS (monoisotopic precursor selection) peptide algorithm was employed but with relaxed restrictions when too few precursors meeting the criteria were found. The fragmentation was performed after accumulation of 2×10^5 ions or after a filling time of 22 ms for each precursor ion (whichever occurred first). MS/MS data were acquired in centroid mode. Only multiply charged (2+ - 7+) precursor ions were selected for MS/MS. Dynamic exclusion was employed with a maximum retention period of 15 s and a relative mass window of 10 ppm. Isotopes were excluded.

For Data Independent Acquisition (DIA), approx. 1 μg of reconstituted peptides were loaded and the same gradient conditions were applied to the LC as for the DDA. The MS conditions were varied as follows: Full scan MS spectra with mass range 350-1650 m/z were acquired in profile mode in the Orbitrap with a resolution of 120,000 FWHM. The filling time was set at a maximum of 20 ms with limitation of 5×10^5 ions. DIA scans were acquired with 34 mass window segments of differing widths across the MS1 mass range with a cycle time of 3 s. HCD fragmentation (30% collision energy) was applied and MS/MS spectra were acquired in the Orbitrap at a resolution of 30,000 FWHM over the mass range 200-2000 m/z after accumulation of 2×10^5 ions or after a filling time of 70 ms (whichever occurred first). Ions were injected for all available parallelizable time. Data were acquired in profile mode. For data acquisition and processing of the raw data the Xcalibur v4.0, Tune v2.1 (Thermo Fisher) were used.

Preparation of skeletal muscles for MS analysis

Tissue lysates (50 μg) were reduced with 10 mM dithiotreitol (Roth #6908.3) for 30 min at 37°C followed by alkylation with 20 mM iodoacetamide (Sigma #I1149) for 30 min at room temperature in the dark. Proteins were precipitated through addition of 100% TCA in a 1:4 volume ratio (Sigma #T6399) for 30 min on ice, spun down at 21,000x *g* for 20 min at 4°C. The pellet was washed twice with 1 mL pre-cooled 10% TCA followed by two washes with 100% ice-cold acetone (Biosolve # 0001037801BS,). The pellets were air-dried before addition of the respective volume of digestion buffer (3M Urea, 100 mM HEPES, pH8) to obtain a protein concentration of 1 – 3 mg/ml. LysC (Wako Chemical GmbH #125- 05061) was added at a ratio of 1:100 (w/w) enzyme:protein and digestion was proceeded for 4 h at 37°C under constant shaking (1000 rpm for 1 h, then 650 rpm). Samples were then diluted 1:1 with MilliQ water and trypsin (Promega #V5111) added at a ratio of 1:100 (w/w) enzyme:protein. Samples were further digested overnight at 37°C under constant shaking (650 rpm). The following day, the digested samples were acidified by addition of TFA (Biosolve #0020234131BS,) in a final concentration of 2% (v/v) and then desalted with Sep Pak C18 cartridges (Waters #WAT054945) according to manufacturer's instructions (Waters Corporation, Milford, MA, USA). The eluates were dried in a speed vacuum centrifuge and dissolved at a concentration of 1 μg/μL in reconstitution buffer (5% (v/v) acetonitrile (Biosolve #0001204102BS), 0.1% (v/v) formic acid (Roth #4724.3) in Milli-Q water). Reconstituted peptides were used for TMT labeling.

TMT labeling

The solution containing the resuspended peptides were brought to a pH 8.5 and a final concentration of 100 mM HEPES (Sigma H3375) prior to labeling. For proteome analysis of the four different muscle types from young, old and geriatric mice, the samples obtained from young mice were used as a common reference. 20 μg of peptides were used for each label reaction. TMT-10plex reagents (Thermo Fisher #90111) were reconstituted in 41 μL of acetonitrile (Biosolve #0001204102BS). TMT labeling was performed in two steps by addition of 2x of the TMT reagent per μg of peptide (e.g., 40 μg of TMT reagent for 20 μg of peptides). TMT reagents were added to samples at room temperature, followed by incubation in a thermomixer (Eppendorf) under constant shaking at 600 rpm for 30 min. After incubation, a second portion of TMT reagent was added and followed by incubation for another 30 min. After checking the labeling efficiency by MS, equal amounts of samples were pooled (200 μg total), desalted using two wells of a Waters Oasis® HLB μElution Plate 30 μm (Waters #186001828BA) and subjected to high pH fractionation prior to MS analysis.

The labeling of the samples was performed as follows:

	young					old					geriatric				
	1	2	3	4	5	1	2	3	4	5	1	2	3	4	5
G	126	127N	127C	128N	128C	129N	129C	130N	130C	131	129N	129C	130N	130C	131
TA	129N	129C	130N	130C	131	126	127N	127C	128N	128C	126	127N	127C	128N	128C
EDL	129N	129C	130N	130C	131	126	127N	127C	128N	128C	126	127N	127C	128N	128C
S	129N	129C	130N	130C	131	126	127N	127C	128N	128C	126	127N	127C	128N	128C

High pH peptide fractionation

Offline high pH reverse phase fractionation was performed using an Agilent 1260 Infinity HPLC System equipped with a binary pump, degasser, variable wavelength UV detector (set to 220 and 254 nm), peltier-cooled autosampler (set at 10°C) and a fraction collector. The column used was a Waters XBridge C18 column (3.5 μm, 100 × 1.0 mm, Waters) with a Gemini C18, 4 × 2.0 mm SecurityGuard

(Phenomenex) cartridge as a guard column. The solvent system consisted of 20 mM ammonium formate (20 mM formic acid (Biosolve #00069141A8BS), 20 mM (Fluka #9857) pH 10.0) as mobile phase (A) and 100% acetonitrile (Biosolve #0001204102BS) as mobile phase (B). The separation was performed at a mobile phase flow rate of 0.1 mL/min using a non-linear gradient from 95% A to 40% B for 91 min. Forty-eight fractions were collected along with the LC separation that were subsequently pooled into 23 or 24 fractions. Pooled fractions were dried in a speed vacuum centrifuge and then stored at −80°C until MS analysis.

Data acquisition of TMT labeled samples

For TMT experiments, fractions were resuspended in 20 μL reconstitution buffer (5% (v/v) acetonitrile (Biosolve #0001204102BS), 0.1% (v/v) TFA in water) and 5 μL were injected into the mass spectrometer. Peptides were separated using the nanoAcquity UPLC system (Waters) fitted with a trapping (nanoAcquity Symmetry C18, 5 μm, 180 μm x 20 mm) and an analytical column (nanoAcquity BEH C18, 2.5 μm, 75 μm x 250 mm). The outlet of the analytical column was coupled directly to an Orbitrap Fusion Lumos (Thermo Fisher Scientific) using the Proxeon nanospray source. Solvent A was water with 0.1% (v/v) formic acid and solvent B was acetonitrile, 0.1% (v/v) formic acid. The samples were loaded with a constant flow of solvent A at 5 μl/min, onto the trapping column. Trapping time was 6 min. Peptides were eluted via the analytical column at a constant flow rate of 0.3 μl/ min, at 40°C. During the elution step, the percentage of solvent B increased in a linear fashion from 5% to 7% in the first 10 min, then from 7% B to 30% B in the following 105 min and to 45% B by 130 min. The peptides were introduced into the mass spectrometer via a Pico-Tip Emitter 360 μm OD x 20 μm ID; 10 μm tip (New Objective) and a spray voltage of 2.2kV was applied. The capillary temperature was set at 300°C. Full scan MS spectra with a mass range of 375-1500 m/z were acquired in profile mode in the Orbitrap with a resolution of 60000 FWHM using the quad isolation. The RF on the ion funnel was set to 40%. The filling time was set to a maximum of 100 ms with an AGC target of 4×10^5 ions and 1 microscan. The peptide monoisotopic precursor selection was enabled along with relaxed restrictions if too few precursors were found. The most intense ions (instrument operated for a 3 s cycle time) from the full scan MS were selected for MS2, using quadrupole isolation and a window of 1 Da. HCD was performed with a collision energy of 35%. A maximum fill time of 50 ms for each precursor ion was set. MS2 data were acquired with a fixed first mass of 120 m/z and acquired in the ion trap in Rapid scan mode. The dynamic exclusion list was set with a maximum retention period of 60 s and a relative mass window of 10 ppm. For the MS3, the precursor selection window was set to the range 400-2000 m/z, with an exclusion width of 18 m/z (high) and 5 m/z (low). The most intense fragments from the MS2 experiment were co-isolated (using Synchronus Precursor Selection = 8) and fragmented using HCD (65%). MS3 spectra were acquired in the Orbitrap over the mass range of 100-1000 m/z and the resolution set to 30000 FWHM. The maximum injection time was set to 105 ms and the instrument was set not to inject ions for all available parallelizable time. For data acquisition and processing of raw data the Xcalibur v4.0 and Tune v2.1 were used.

Affinity purification of Smoc2-GFP fusion protein

For generation of stable lines expressing either Smoc2-GFP or GFP control, plasmids were generated using the Gateway Technology (Invitrogen). The destination vector containing GFP was combined with the entry clone (vector generated with pDONR) Smoc2 (Dharmacon #MMM1013-202764967). The X-tremeGENE9 DNA transfection reagent (Sigma-Aldrich) was then used to stably transfect the HEK293 (Flp-In 293 T-Rex cells) cells.

To induce the expression of either GFP or Smoc2-GFP, cells were cultured until they reached a confluency of 70%, then tetracycline (1 μg/ml, Sigma, #87128) was added. 48 h after induction cells were harvested by trypsinization and the cell pellet was frozen at −80°C. The cells were lysed in 200 μl RIPA buffer (150 mM Sodium Chloride, 0.5% Sodium Deoxycholate, 0.1% SDS, 50 mM Tris pH8, 1% Triton X-100, Phosstop (Roche #4906837001), complete PI (Roche #11697498001)), and the pulldown was performed using GFP-traps according to manufacturer's instructions (Chromotek #gta-100). Immunoblot analysis was performed on 10% of the sample to show Smoc2-GFP fusion-protein expression. Sample preparation for mass spectrometry analysis included sonication for 10x 1 min on, 30 s off at 20°C and highest intensity settings in a Bioruptor Plus and boiling 10 min at 95°C, followed by reduction with 10 mM dithiotreitol (Roth #6908.3) for 30 min at 37°C and alkylation with 20 mM iodoacetamide (Sigma #I1149) for 30 min at room temperature in the dark. Proteins were precipitated through addition of 1:8 volume of 100% Acetone (Biosolve #0001037801BS) over night at −20°C. "Protein precipitation, digestion and desalting were performed as described in "Preparation of MuSCs and FAPs for MS analysis."

Data acquisition for GFP-trap samples

Digested peptides were separated using the nanoAcquity UPLC system (Waters) fitted with a trapping (nanoAcquity Symmetry C_{18}, 5μm, 180 μm x 20 mm) and an analytical column (nanoAcquity BEH C_{18}, 1.7μm, 75μm x 250mm). The outlet of the analytical column was coupled directly to an Orbitrap Fusion Lumos (Thermo Fisher Scientific) using the Proxeon nanospray source. Solvent A was water with 0.1% (v/v) formic acid and solvent B was acetonitrile with 0.1% (v/v) formic acid. The samples (500 ng) were loaded with a constant flow of solvent A at 5 μl/min onto the trapping column. Trapping time was 6 minutes. Peptides were eluted via the analytical column with a constant flow of 0.3 μl/ min. During the elution step, the percentage of solvent B increased in a linear fashion from 3% to 25% in the first 30 minutes, then increased to 32% in the following 5 minutes and finally to 50% in the last 0.1 minutes. Total runtime was 60 minutes. The peptides were introduced into the mass spectrometer via a Pico-Tip Emitter 360 μm OD x 20 μm ID; 10 μm tip (New Objective) and a spray voltage of 2.2 kV was applied. The capillary temperature was set at 300°C. The RF lens was set to 30%. Full scan MS spectra with mass range 375-1500 *m/z* were acquired in profile mode in the Orbitrap with a resolution of

120000 FWHM. The filling time was set to a maximum of 50 ms with a limitation of 2×10^5 ions. The "Top Speed" method was employed to take the maximum number of precursor ions (with an intensity threshold of 5×10^3) from the full scan MS for fragmentation (using HCD collision energy, 30%) and quadrupole isolation (1.4 Da window) and measurement in the ion trap, with a cycle time of 3 s. The MIPS (monoisotopic precursor selection) peptide algorithm was employed but with relaxed restrictions when too few precursors meeting the criteria were found. The fragmentation was performed after accumulation of 2×10^3 ions or after a filling time of 300 ms for each precursor ion (whichever occurred first). MS/MS data were acquired in centroid mode, with the Rapid scan rate and a fixed first mass of 120 *m/z*. Only multiply charged (2^+ - 7^+) precursor ions were selected for MS/MS. Dynamic exclusion was employed with a maximum retention period of 60 s and a relative mass window of 10 ppm. Isotopes were excluded. Additionally, only 1 data dependent scan was performed per precursor (only the most intense charge state selected). Ions were injected for all available parallelizable time. In order to improve the mass accuracy, a lock mass correction using a background ion (*m/z* 445.12003) was applied. For data acquisition and processing of the raw data, the Xcalibur 4.0 (Thermo Scientific) and Tune version 2.1 were employed.

Parallel reaction monitoring for Smoc2

Seven peptides belonging to Smoc2 were selected and their isotopically labeled versions (C-terminal heavy Arginine (U-13C6; U-15N4) or Lysine (U-13C6; U-15N2)) were synthesized by JPT Peptide Technologies GmbH (Berlin, Germany). Peptides were reconstituted in 20% (v/v) acetonitrile (Biosolve #0001204102BS), 0.1% (v/v) formic acid (Roth #4724.3) and further pooled together in a 1:1 ratio. An aliquot of the pooled peptides, corresponding to approximatively 17.14 fmol per peptide, was analyzed by both DDA and DIA MS analysis and used for assay generation using Spectrodive v.9 (Biognosys AG, Schlieren, Switzerland).

Peptides were analyzed using a nanoAcquity UPLC system (Waters) fitted with a trapping (nanoAcquity Symmetry C18, 5 μm, 180 μm x 20 mm) and an analytical column (nanoAcquity BEH C18, 2.5 μm, 75 μm x 250 mm), and coupled to an Orbitrap Fusion Lumos (Thermo Fisher Scientific, Waltham, MA, USA). Solvent A was water with 0.1% (v/v) formic acid and solvent B was acetonitrile with 0.1% (v/v) formic acid. Peptides were eluted via the analytical column with a constant flow of 0.3 μl/min. During the elution step, the percentage of solvent B increased in a non-linear fashion from 0% to 40% in 40 min. Total runtime was 60 min, including clean-up and column re-equilibration. PRM acquisition was performed in a scheduled fashion for the duration of the entire gradient (after instrument calibration in an unscheduled mode) using the ''DIA'' mode with the following settings: resolution 120,000 FWHM, AGC target 3×10^6, maximum injection time (IT) 250 ms, isolation window 0.4 m/z. For each cycle, a ''full MS'' scan was acquired with the following settings: resolution 120,000 FWHM, AGC target 3×10^6, maximum injection time (IT) 10 ms, scan range 350 to 1650 m/z.

Sample preparation for phosphoproteomics analysis

Lysates (corresponding to 50 μg of protein extract) from C2C12 treated with Smoc2 were acetone precipitated, digested into peptides and desalted, as described in "Preparation of MuSCs and FAPs for MS analysis". The last desalting step was performed using 50 μl of a 80% ACN and 0.1% TFA buffer solution. Before phosphopeptide enrichment, samples were filled up to 210 μl using 80% ACN and 0.1% TFA buffer solution. Phosphorylated peptides were enriched using Fe(III)-NTA cartridges (Agilent Technologies #G5496-60085) using the AssayMAP Bravo Platform (Agilent Technologies), as described in Post et al. (2017). Briefly, Fe(III)-NTA cartridges were washed with 250 μL of 100% ACN/0.1% TFA and conditioned using 250 μl of loading buffer consisting of 80% ACN and 0.1% TFA. After loading the samples into the cardridge, the columns were washed with 250 μl of loading buffer, and then the phosphopeptides were eluted with 25 μl of 1% ammonia directly into 25 μl of 10% FA in water. Samples were dried down with a speed vacuum centrifuge and stored at −20 °C until MS analysis.

Data independent acquisition for enriched phosphopeptides

Prior to analysis, samples were reconstituted in 5% ACN, 95% Milli-Q water, with 0.1% FA and spiked with iRT peptides (Biognosys, Switzerland). Peptides were separated in trap/elute mode using the nanoAcquity MClass Ultra-High-Performance Liquid Chromatography system (Waters, Waters Corporation, Milford, MA, USA) equipped with a trapping (nanoAcquity Symmetry C18, 5 μm, 180 μm × 20 mm) and an analytical column (nanoAcquity BEH C18, 1.7 μm, 75 μm × 250 mm). Solvent A was water and 0.1% formic acid, and solvent B was acetonitrile and 0.1% formic acid. Between 40 and 80% of the samples were loaded with a constant flow of solvent A at 5 μl/min onto the trapping column. Trapping time was 6 min. Peptides were eluted via the analytical column with a constant flow of 0.3 μl/min. During the elution step, the percentage of solvent B increased in a nonlinear fashion from 0%–40% in 60 min. For MS analysis, either a Q exactive HF-X (Thermo Fisher Scientific, Bremen, Germany) or an Exploris 480 (Thermo Fisher Scientific, Bremen, Germany) mass spectrometer were used. The MS were coupled to the LC using the Proxeon nanospray source. The peptides were introduced into the mass spectrometer via a Pico-Tip Emitter 360-μm outer diameter × 20-μm inner diameter, 10-μm tip (New Objective) heated at 300°C, and a spray voltage of 2.2 kV was applied. The capillary temperature was set at 300°C.

For analysis on the Q Exactive HF-X, the radio frequency ion funnel was set to 40%. For DIA data acquisition, full scan MS spectra with mass range 350–1650 m/z were acquired in profile mode in the Orbitrap with resolution of 120,000 FWHM. The default charge state was set to 3+. The filling time was set at maximum of 60 ms with limitation of 3×10^6 ions. DIA scans were acquired with 30 mass window segments of differing widths across the MS1 mass range. Higher collisional dissociation fragmentation (stepped normalized collision energy; 25.5, 27, and 30%) was applied and MS/MS spectra were acquired with a resolution of 30,000 FWHM with a fixed first mass of 200 m/z after accumulation of 3×10^6 ions or after filling time of 47 ms (whichever occurred first). Data were acquired in

profile mode. For data acquisition and processing of the raw data, Xcalibur 4.0 (Thermo Fisher) and Tune version 2.9 were used.

For analysis on the Exploris 480, the radio frequency ion funnel was set to 30%. For DIA data acquisition, full scan MS spectra with mass range 350–1650 m/z were acquired in profile mode in the Orbitrap with resolution of 120,000 FWHM. The default charge state was set to 3+. The filling time was set at maximum of 60 ms with limitation of 3×10^6 ions. DIA scans were acquired with 30 mass window segments of differing widths across the MS1 mass range. Higher collisional dissociation fragmentation (stepped normalized collision energy; 25.5, 27, and 30%) was applied and MS/MS spectra were acquired with a resolution of 30,000 FWHM with a fixed first mass of 200 m/z after accumulation of 3×10^6 ions or after filling time of 47 ms (whichever occurred first). Data were acquired in profile mode. For data acquisition and processing of the raw data, Xcalibur 4.4 (Thermo Fisher) and Orbitrap Exploris 480 Tune version 2.0 were used.

Immunofluorescence analysis of cryo-sections

TA muscles were isolated, cut in the mid-belly region, frozen in freezing medium (v/v: 1:3 30% Sucrose (Affymetrix #21938) and Thermo Scientific Richard-Allan Scientific Neg-50 Frozen Section Medium (Thermo Fisher #6502) in liquid nitrogen and stored at −80°C. Cryosections of the TA muscles (14 μm thick) were fixed with 2% formaldehyde (Roth #4979.1) in PBS for 5 min at room temperature, washed twice with PBS and then permeabilized (0.1% Triton X-100 (Roth #3051.3), 0.1 M Glycine (VWR #1042011000) in PBS) for 5 min at room temperature. Washing with PBS was repeated twice and cryo sections were incubated with blocking solution for 1 h at room temperature. For Pax7 staining, the Mouse on Mouse Blocking Reagent (Vector #MKB-2213, 1:40 in PBS) was used for 1 h at room temperature. For all other stainings, 5% horse serum (Thermo Fisher #26050-088) in PBS was used as blocking solution. The sections were incubated at 4°C overnight with primary antibodies against the following proteins: Col14a1 (Abcam #ab101464, 1:100), devMHC (Hybridoma clone F.1652, mouse IgG1, undiluted), Elastin (Abcam #ab217356, 1:100), Laminin (Sigma #L9393, Rabbit IgG, 1:1000), Pax7 (Pax7, DSHB, Hybridoma mouse IgG1, undiluted), Pdgfrα (R&D #AF1062, 1:100), Smoc2 (MyBiosource #MBS2527784, rabbit IgG, 1:100). After washing three times with PBS, the sections were incubated for 1 h at room temperature with the respective secondary antibody: anti-goat IgG (Alexa Fluor 647, #A-21447), anti-mouse IgG1 (Alexa Fluor 546, #A-21123), anti-rabbit IgG (Alexa Fluor 488, #A-21206), anti-rabbit IgG (Alexa Fluor 546, #A10040), anti-rat IgG (Alexa Fluor 488, #A-21208), all from Thermo Fisher Scientific, 1:1000 in 5% horse serum in PBS. After washing, nuclei were stained with Hoechst (1:2500 in PBS) at room temperature for 5 min followed by three washing steps using PBS and mounting in Permafluor mounting medium (Thermo Fisher #TA-006-FM). Microscopy was performed with an Axio Imager.Z2 equipped with a Plan-Apochromat 20x/0.8 M27 Objective (Zeiss, resolution: 0.227 μm x 0.227 μm per pixel) using the ZEN software v3.0 (Zeiss). For displaying images, adjustments of individual color channels were made in the same way for all the images belonging to the same experiment.

Sirius red staining

Muscle cryosections were fixed for 5 min at room temperature with 2% PFA and washed three times with PBS. Pico-sirius red staining (Direct Red 80 (Sigma #365548-5G)) in picric acid solution (Sigma #P6744-1GA)) was performed for 1 h at room temperature and slides were washed subsequently two times with acidified water (0.5% acetic acid (Roth #6755.1) in water). Most of the water was removed, samples were rinsed in Xylene (Sigma #534056) and mounted in Xylene-containing mounting medium (Leica #14046430011). Microscopy was performed with an Axio Imager.Z2 equipped with a Plan-Apochromat 20x/0.8 M27 Objective (Zeiss, resolution: 0.227 μm x 0.227 μm per pixel) using the ZEN software v3.0 (Zeiss).

Floating myofiber culture

Fiber culture isolation was performed as described in Hüttner et al. (2019). Briefly, single myofibers were isolated from EDL muscles of C57BL/6J mice by incubating the EDL muscle for 60-120 min in 0.2% collagenase (Sigma #C0130) in DMEM (Sigma #D6429). Single myofibers were separated using a large bore Pasteur pipette with a fire-rounded opening hole in isolation medium (20% FBS (Thermo Fisher #10270106) in DMEM). Isolated myofibers (ca. 50 per condition) were then either fixed and used for immunofluorescence staining immediately as described in "Immunofluorescence of floating myofibers" or incubated for 32h or 72h in culture medium (20% FBS, 1% chicken embryo extract (Seralab, CE-650-J) in DMEM). Smoc2 application was performed with 5 μg/ml Smoc2 recombinant protein (R&D Systems #6075-SM-050) directly after isolation. Transfection with siRNA targeting Itgb1 (Dharmacon #L-040783-01-0005) or a non-targeting control (Dharmacon #D-001810-10-05) was performed 4 h after isolation using the RNA-iMAX transfection reagent according to the instructions provided by the manufacturer (Thermo Scientific). After respective times of incubation, myofibers were fixed for immunofluorescence analysis as described in "Immunofluorescence of floating myofibers." For qPCR analysis, living myofibers were harvested in a 1.5 mL tube, excess medium was removed and 1 mL TriFast (Peqlab) was added for RNA isolation.

Immunofluorescence of floating myofibers

Single myofibers were fixed in 2% formaldehyde (Roth #CP10.1) in PBS for 5 min at room temperature, washed twice with PBS and permeabilized with permeabilization solution (0.1% Triton X-100 (Roth #3051.3), 0.1 M Glycine (VWR #1042011000) at room temperature for 10 min. Washing with PBS was repeated twice and the myofibers were incubated in blocking solution (for Bcam: 5% horse serum (Thermo Fisher #26050-088) and 0.3% Triton X-100 in PBS, for all other antibodies: 5% horse serum in PBS) for 1 h at room temperature. Incubation with primary antibodies was carried out in 5% horse serum in PBS overnight at 4°C using antibodies against the following proteins: Calcr (Biorad #AHP635, rabbit IgG, 1:100), Itgb4 (abcam #ab236251, rabbit IgG, 1:200), MyoD (Merck

#MABE132, rat IgG2a, 1:100), Pax7 (Pax7, DSHB, Hybridoma mouse IgG1, undiluted), Sun2 (Atlas antibodies #HPA001209, rabbit IgG, 1:500). For immunostainings against Bcam and Pax7, one part of antiboby against Bcam (R&D #AF8299, goat IgG, 1:25) was mixed with one part of Pax7 hybridoma antibody and one part of antibody dilution buffer (1% BSA (Thermo Fisher #23209) and 0.3% Triton X-100 in PBS)). After washing three times with PBS the respective secondary antibodies were added for 1 h at room temperature: anti-goat IgG (Alexa Fluor 647, #A-21447), anti-mouse IgG1 (Alexa Fluor 546, #A-21123), anti-rabbit IgG (Alexa Fluor 488, #A-21206), anti-rabbit IgG (Alexa Fluor 546, #A10040), anti-rat IgG (Alexa Fluor 488, #A-21208), all from Thermo Fisher Scientific, 1:1000 in 5% horse serum in PBS. After washing, nuclei were stained with Hoechst (1:2500 in PBS) at room temperature for 5 min, followed by an additional washing step and mounting in Permafluor mounting medium (Thermo Fisher #TA-006-FM). Microscopy was performed with an Axio Imager.Z2 equipped with a Plan-Apochromat 40x/1.3 Oil DIC (UV) VIS IR M27 Objective using Apotome mode. For quantification cells were outlined using ZEN software v3.0 (Zeiss) and the sum intensity was used.

Proximity labeling assay of MuSCs on floating fiber culture

Freshly isolated myofibers were fixed with 2% PFA for 10 min at room temperature, washed twice with PBS followed by permeabilization with 0.1 M glycine, 0.1% Triton X-100 in PBS (pH 7.4) for 10min at room temperature. After incubation with Duolink blocking solution (Sigma-Aldrich, #DUO92101) for 1h at room temperature, myofibers were incubated with mouse anti-PAX7 (DSHB) at 4°C overnight. Samples were washed with PBS and stained with secondary antibodies (Alexa Fluor mIgG1 488, # A-21121; ThermoScientific) for 1h at room temperature. The proximity ligation assay (PLA) was performed using the Duolink *In Situ* Detection Reagents Red (Sigma-Aldrich, #DUO92101) according to the manufacturer's protocol. Primary antibodies were directly coupled by using the Duolink *In Situ* Probemaker MINUS and POSITIVE (Sigma-Aldrich; #DUO92010 and #DUO92009). Primary antibodies used were: mouse anti-ITGB1 (Sigma-Aldrich, MA5-17103) and mouse anti-Smoc2 (Santa Cruz, sc-376104). Images were taken with an Axio Observer.D1 microscope equipped with a 63x objective and analyzed with the ZEN software v3.0 (Zeiss).

qRT-PCR

RNA isolation was performed with TriFast (Peqlab) according to manufacturer's protocol. Myofibers were homogenized in TriFast by pipetting them up and down for 3 min and vortexing. Cells were either directly harvested into TriFast or cell pellets were resuspended and lysed by pipetting up and down for 3 min and vortexing. Reverse transcription was performed on 600 ng total RNA. RT-qPCR was performed on a CFX384 Touch RealTime PCR System (Biorad) using SyBrGreen (Biorad). Technical triplicates were performed for each sample. For triplicates having a Cq-SEM (calculated by Bio-Rad CFX Manager 3.1) higher than 0.4, the replicate with the largest difference was excluded. The list of primers used can be found in Table S8.

Immunoblot analysis

Skeletal muscles were homogenized and lysed as described in "Tissue lysis for immunoblot and MS analysis." C2C12 cells were lysed in RIPA buffer for 20 min on ice and sonicated using a Bioruptor for 10x 1 min on, 30 s off at 20°C and highest intensity settings. Then, 10 μg protein was separated on 4%–20% Mini-PROTEAN® TGX Precast Protein Gels (Biorad #4561094) and blotted onto a Roti®-NC Transfermembrane (Roth #HP40.1). Proteins were visualized with Ponceau S staining before incubation with 3% BSA (Thermo Fisher # 23209) in TBST for 1 h at room temperature. Membranes were then incubated with the respective primary antibodies in 3% BSA, 0.05% NaAc in TBST overnight at 4°C using antibodies against the following proteins: Smoc2 (Santa Cruz #sc-376104, mouse, 1:250), Gapdh (Santa Cruz #sc-365062, mouse, 1:200), Erk1 (Santa Cruz #sc-271269, mouse, 1:1500), Erk2 (Santa Cruz #sc-1647, mouse, 1:1500), pErk1/2 (Cell signaling #4370, rabbit, 1:2000). On the next day, the membranes were washed three times for 10 min in TBST and incubated for 1 h at room temperature with the respective HRP coupled secondary antibodies: goat anti-rabbit immunoglobulins-HRP (Dako #P0448, 1:1000), goat anti-mouse immunoglobulins-HRP (Dako #P0447, 1:1000)). After washing with TBST the membranes were incubated with Pierce ECL Western Blotting Substrate (Thermo Fisher #32209) and detection was carried out using a ChemiDocTM XRS+ Imaging system (Biorad). Quantification was performed in ImageJ v1.59n.

Cardiotoxin muscle injury and Smoc2 treatment

Mice were anesthetized by constant inhalation of Isoflurane. The TA muscles were injured either once or three times every 14 days by injecting 50 μl of 20 μM Cardiotoxin (Latoxan #L8102) in sterile 0.9% NaCl per TA muscle. Smoc2 recombinant protein (R&D Systems #6075-SM-050) was injected twice after each injury (10 μg Smoc2 in 50 μl sterile 0.9% NaCl) three and five days after the respective Cardiotoxin injection. Metacam (1 mg/kg) was used for pain relief, administered s.c. on the day of injury as well as two following days.

Decellularization of TA tissue

Isolated TA muscles were cut in the transverse plane in 4 equally sized pieces. The two middle pieces were used for analysis. On one of the pieces the protocol of Silva et al. (2016) was used for decellularization. Successful decellularization was tested by comparing DNA levels in native (not decellularized) and decellularized tissues. Briefly, decellularized and native tissues were digested in papain enzyme digestion solution (3.88 units/ml Papain, 100 mM L-cysteine (Sigma #A91565), 100 mM Sodium phosphate (Sigma #S0876), 5 mM EDTA (Roth #8043.3), pH 6.5) for 18 h at 60°C under constant shaking (650 rpm). After vortexing, the samples were spun down at 650x *g* for 1 min and DNA amounts were quantified using the DNA Quantitation Kit (Sigma #DNAQF) according to manufacturer's instructions. Decellularized muscles were further processed for mass spectrometry analysis as described for whole tissue.

QUANTIFICATION AND STATISTICAL ANALYSIS

Data processing for DIA samples

For MuSCs, the DIA spectral library was generated using DDA data searched with MaxQuant (version 1.5.3.30) (Cox and Mann, 2008). The data were searched against a species specific Uniprot database (*Mus musculus,* reviewed entry only, release 2016_01) with a list of common contaminants appended using the Andromeda search engine (Cox et al., 2011). The data were searched with the following modifications: Carbamidomethyl (C) (fixed) and Oxidation (M) and Acetyl (Protein N-term) (variable). The mass error tolerance for the full scan MS spectra was set at 20 ppm and for the MS/MS spectra at 0.5 Da. A maximum of 2 missed cleavages were allowed. The library search was set to a 1% false discovery rate (FDR) at both, the protein and the peptide level. The spectral library was generated using Spectronaut v10 (Biognosys) using the MaxQuant output. The library contained 127,689 precursors, corresponding to 5,645 protein groups using Spectronaut protein inference. DIA data were analyzed and searched against the specific spectral library using Spectronaut v10. Relative quantification was performed in Spectronaut for each pairwise comparison using the replicate samples from each condition and default settings. The data (candidate table) and protein quantity data reports were then exported, and further data analyses and visualization were performed using R. Proteins with $q < 0.05$ and absolute $\log_2$ fold change > 0.58 were considered as significantly affected.

For FAPs, a DpD (DDA plus DIA) library was created by searching DIA and DDA runs from the same samples using Spectronaut Pulsar v14 (Biognosys). The data were searched against a species specific Uniprot database (*Mus musculus,* reviewed entry only, release 2016_01) with a list of common contaminants appended. The data were searched with the following modifications: carbamidomethyl (C) as fixed modification, and oxidation (M), acetyl (protein N-term) as variable modifications. A maximum of 2 missed cleavages was allowed. The library search was set to 1% false discovery rate (FDR) at both protein and peptide levels. This library contained 87,314 precursors, corresponding to 5,165 protein groups using Spectronaut protein inference. DIA data were then uploaded and searched against this spectral library using Spectronaut Professional (v.14) and default settings. Protein quantities were exported from Spectronaut and used to assess the abundance of Smoc2 following Monensin treatment.

Data processing for TMT labeled samples

TMT-10plex data were processed using Proteome Discoverer v2.0 (Thermo Fisher). Data were searched against the relevant species-specific fasta database (Uniprot database, Swissprot entry only, release 2016_01 for *Mus musculus*) using Mascot v2.5.1 (Matrix Science) with the following settings: enzyme was set to trypsin, with up to 1 missed cleavage. MS1 mass tolerance was set to 10 ppm and MS2 to 0.5 Da. Carbamidomethyl cysteine was set as a fixed modification and oxidation of Methionine as variable. Other modifications included the TMT-10plex modification from the quantification method used. The quantification method was set for reporter ions quantification with HCD and MS3 (mass tolerance, 10 ppm). The false discovery rate for peptide-spectrum matches (PSMs) was set to 0.01 using Percolator (Brosch et al., 2009).

Reporter ion intensity values for the PSMs were exported and processed with procedures written in R (v. 3.4.1), as described in Heinze et al. (2018). Briefly, PSMs mapping to reverse or contaminant hits, or having a Mascot score below 15, or having reporter ion intensities below 1×10^3 in all the relevant TMT channels were discarded. TMT channels intensities from the retained PSMs were then $\log_2$ transformed, normalized and summarized into protein group quantities by taking the median value. At least two unique peptides per protein were required for the identification and only those peptides with one missing value across all 10 channels were considered for quantification. Protein differential expression was evaluated using the limma package (Ritchie et al., 2015). Differences in protein abundances were statistically determined using an unpaired Student's t test moderated by the empirical Bayes method. P values were adjusted for multiple testing using the Benjamini-Hochberg method (FDR, denoted as "adj p") (Benjamini and Hochberg, 1995). Proteins with adj $p < 0.05$ were considered as significantly affected.

Data processing for GFP-trap analysis

The MaxQuant software (version 1.5.3.28) was used to search the data. The data were searched against a species-specific database (Uniprot database, Swissprot entry only, release 2016_01 for *Homo sapiens*) with a list of common contaminants appended. The data were searched with the following modifications: Carbamidomethyl (C) (fixed) and Oxidation (M) and Acetyl (Protein N-term) (variable). The mass error tolerance for the full scan MS spectra was set at 20 ppm and for the MS/MS spectra at 0.5 Da. A maximum of 2 missed cleavages was allowed. Peptide and protein level 1% FDR were applied using a target-decoy strategy (Elias and Gygi, 2007). Peptide counts were exported from the protein groups output table of MaxQuant.

PRM analysis for quantification of Smoc2

Peak group identification and quantification was performed using SpectroDive v9. Quantification was performed using a spike-in approach. Thereby, the summed height of all the identified transitions was used to estimate the quantity of each peptide.

Protein Access	GeneID	Peptide sequence	Charge state
Q8CD91	Smoc2	LSEPDPSHTLEER	+2, +3
Q8CD91	Smoc2	FSALTFLR	+2
Q8CD91	Smoc2	DPQLEIAHR	+2, +3

Peptide quantities were normalized across samples by dividing for the integrated intensity of the Base Peak Chromatogram extracted for each sample from ''full MS'' scans using Xcalibur v4.1 (Thermo Fisher Scientific, Waltham, MA, USA). Further, the ratio between the heavy peptide (known concentration spiked-in) and light peptide was used to estimate the absolute amount of Smoc2 per μg of lysate. For calculating the total amount of Smoc2 per TA muscle the molecular weight of Smoc2 was assumed to be 47.647 kDa. One TA muscle homogenized and lysed as described in ''Tissue lysis for immunoblot and MS analysis'' and assumed to have a total volume of 700 μl after homogenization.

Data processing for phosphoproteomics

Raw data were analyzed using the directDIA pipeline in Spectronaut v.13 (Biognosys). The data were searched against a species specific (Uniprot database, Swissprot entry only, release 2016_01 for *Mus musculus*) and a common contaminants database. The data were searched with the following modifications: Carbamidomethyl (C) (Fixed) and Oxidation (M), Acetyl (Protein N-term), Phospho (STY) (Variable). PTM localization probability was set to 0.75. A maximum of 2 missed cleavages for trypsin and 5 variable modifications were allowed. The identifications were filtered to satisfy a FDR of 1% on peptide and protein level. Peptide report was exported from Spectronaut and further processed with R (v.3.6.3) and R studio server (v. 1.2.5042) using in-house pipelines and scripts. Phosphosite level intensities were derived by summing the intensities of all precursors containing a given phosphosite. Phosphosite intensities were log2 transformed and normalized by quantile normalization using preprocessCore library (Bolstad et al., 2003). Differences in phosphosite levels were statistically determined using a paired Student's t test moderated by the empirical Bayes method, as implemented in the limma package (Ritchie et al., 2015). False discovery rate was estimated using *fdrtool* (Strimmer, 2008).

Quantification of IF stainings from TA muscles

Quantification of Col14a1 and Elastin on TA muscle sections was performed on a defined area for each muscle: 0.54 mm^2 for Col14a1 and 1.349 mm^2 for Elastin using the sum intensity measured by Zen 3.0 using the raw images. The number of Pax7+ MuSCs was measured in the regenerating area. The percentage of myofibers expressing devMHC was measured by counting all devMHC expressing and non-devMHC expressing fibers in the injured area. The myofiber diameter was measured as the minimal fiber feret. Significance was tested using an unpaired two-tailed Student's t test after testing for normal distribution using the Shapiro Wilk normality test, and indicated as: $*p < 0.05$, $**p < 0.01$, $***p < 0.001$, n.s. = not significant, unless otherwise stated.

Quantification of IF stainings on floating myofibers

Quantification of Bcam, Calcr, Itgb4 and Sun2 was performed by outlining the entire cell and analysis of the sum intensity measured by Zen 3.0 using the raw images. Significance was tested using an unpaired two-tailed Student's t test after testing for normal distribution using the Shapiro Wilk normality test, and indicated as: $*p < 0.05$, $**p < 0.01$, $***p < 0.001$, n.s. = not significant, unless otherwise stated.

Quantification of immunoblots

Smoc2 and Asporin quantification in young, old and geriatric muscles was performed using ImageJ using the raw images acquired. Chemiluminescence intensity acquired with the respective antibodies was normalized to the respective chemiluminescence intensity reflecting GAPDH amounts for each sample separately. The pERK to ERK ratio was also measured using ImageJ. Smoc2 expression in regenerating TA muscles was normalized to total protein amount, obtained by Ponceau S staining and measured using Image Lab v6.0.1. Significance was tested by using a one-way ANOVA and indicates as: $*p < 0.05$, $**p < 0.01$, $***p < 0.001$, n.s. = not significant, unless otherwise stated.

Ingenuity pathway analysis for MuSCs proteome data

Candidate tables from Spectronaut were used as input for canonical pathways and upstream regulator analyses using Ingenuity Pathway Analysis software v.01-14 (QIAGEN Inc.). A significant cut-off of $q < 0.05$ was applied.

Analysis and integration of micro array transcriptome data

The following steps were conducted in R (version 3.3.3). Datasets with the accessions GSE63860 (Alonso-Martin et al., 2016), GSE47177 (Liu et al., 2013), GSE47401 (Price et al., 2014) and GSE81096 (Lukjanenko et al., 2016) were downloaded from GEO. Each dataset was annotated with either the R packages mouse4302.db (for GSE63860) or mogene10sttranscriptcluster.db (for GSE47177 and GSE47401) or illuminaMousev2.db (for GSE81096) to obtain gene symbols and additional meta data. Differential expression on the probe level was evaluated using the R package limma (version 3.30.13) (Ritchie et al., 2015). For GSE81096 the probes with the quality value ''Bad,'' ''No match'' or ''NA'' were removed prior to further analysis steps. Differences in mRNA abundances were statistically determined using unpaired Student's t test moderated by the empirical Bayes method. P values were adjusted for multiple testing using the Benjamini-Hochberg method (FDR, denoted as ''adj p'') (Benjamini and Hochberg, 1995). In case of multiple probes per gene symbol, the probe with the lowest adj p was chosen. Transcripts with adj $p < 0.05$ and absolute log_2 fold change > 0.58 were considered as significantly affected.

Analysis and integration of RNaseq transcriptome data

RNA sequencing reads of quiescent CD34-High and CD34-Low satellite cells isolated from young and geriatric WT mice (16 samples with the GEO accessions GSM4770480 to GSM4770495 from project GSE157562) as well as reads from satellite cells of young and aged control mice (6 samples with the Short Read Archive accessions SRR7965941, SRR7965942, SRR7965943, SRR7965949, SRR7965950 and SRR7965951 from project PRJNA494728) were downloaded and mapped using STAR (Dobin et al., 2013) (version 2.7.6a, parameters:–alignIntronMax 100000,–outSJfilterReads Unique,–outSAMmultNmax 1,–outFilterMismatchNoverLmax 0.04) to the mouse genome (*Mus musculus*, GRCm38) using Ensembl genome annotation (Release 100). Read counting for summarization was done with FeatureCounts (version 1.6.5, multi-mapping or multi-overlapping reads were not counted, stranded mode was set to "–s 0") (Liao et al., 2014). Differentially expressed genes (DEGs) were determined with R (version 4.0.3) using the DESeq2 package (version 1.30.0) (Love et al., 2014). For each gene in each comparison, the p value was calculated using the Wald significance test. Resulting p values were adjusted for multiple testing using the Benjamini & Hochberg correction. The $\log_2$ fold change values were shrunk with the function DESeq2::lfcShrink() to control for variance of fold change estimates for genes with low read counts. Transcripts with adj $p < 0.05$ and absolute $\log_2$ fold change > 0.58 were considered differentially expressed.

For comparing the micro array data, the RNaseq datasets and the proteomics results of this study all data were combined based on the gene symbols.

Analysis of cellular compartments in aging skeletal muscles

Normalized protein intensities obtained from the proteomic data were analyzed using a Compartment Normalized Value analysis, as described in Parca et al. (2018). Cellular compartments were defined using the follow Gene Ontology Cellular Component terms and their children terms:

Compartment	GO term
Nucleus	GO:0005634
Cytosol	GO:0005737
Mitochondrion	GO:0005739
Extracellular	GO:0005576, GO:0031012, GO:0044421, GO:0044420
Peroxisome	GO:0005777
Lysosome	GO:0005764
ER	GO:0005783
Golgi	GO:0005794
Membrane	GO:0005886
Cytoskeleton	GO:0005856

Analysis and integration of scRNaseq data

The data from Giordani et al. (2019) was downloaded from NCBI Gene Expression Omnibus (GEO) (Edgar et al., 2002) (accession GSE110878). Using the cell type labels assigned by the original authors, an scfind object was constructed (Lee et al., 2019). The selected 67 ECM proteins affected by aging were queried individually against the index and the enrichment as defined by a hypergeometric test, as displayed in Figure 3E. For each gene, scfind identifies the cell type c with the highest enrichment using a hypergeometric test. For the hypergeometric test, the number of successes is given by the number of cells expressing the gene of interest, the number of failures by the number of cells not expressing the gene, and the number of draws corresponds to the number of cells in c. A p value is calculated based on the observed number of cells in c that express the gene of interest.

Network analysis of secreted ligands affected by aging in skeletal muscles and their receptors expressed by MuSCs

The network was constructed using the ligand-receptors interactions obtained from Ramilowski et al. (2015) using Cytoscape v.3.8.0 (Shannon et al., 2003). We selected all the ECM/secreted proteins (as defined for the compartment analysis, see above) as aging-affected ligands that were affected in at least one muscle type at old age. We selected as receptors expressed by MuSCs all the genes that were detected in at least one of the following MuSC transcriptomics experiments: GSE63860 (Alonso-Martin et al., 2016), GSE47177 (Liu et al., 2013), GSE47401 (Price et al., 2014) and GSE81096 (Lukjanenko et al., 2016). In total, the network contained 100 ligands and 243 receptors and it is reported in Table S4. Network visualization shown in Figures 4A and S7A was performed using the app enhancedGraphics (Morris et al., 2014).